

Tectonics*

RESEARCH ARTICLE

10.1029/2022TC007726

Key Points:

- · Pre-rift basement fabrics beneath the Tanganyika rift are dominated by NW and NNE trends, parallel to the rift faults
- Gravity-magnetic modeling of the basin reveals intra-basement shear zone exploited by large-offset earlyrift intrabasinal fault
- Although inherited basement structure modulated the earliest rift faulting, the effect cascaded through to subsequent phases of extension

Supporting Information:

Supporting Information may be found in the online version of this article.

Correspondence to:

S. N. Shaban. snshaban@syr.edu

Citation:

Shaban, S. N., Kolawole, F., & Scholz, C. A. (2023). The deep basin and underlying basement structure of the Tanganyika Rift. Tectonics, 42, e2022TC007726. https://doi.org/10.1029/2022TC007726

Received 23 DEC 2022 Accepted 13 JUN 2023

Author Contributions:

Conceptualization: Shaidu N. Shaban, Christopher A. Scholz Data curation: Shaidu N. Shaban,

Folarin Kolawole

Formal analysis: Shaidu N. Shaban Funding acquisition: Christopher A. Scholz Investigation: Shaidu N. Shaban, Folarin

Kolawole, Christopher A, Scholz Methodology: Shaidu N. Shaban, Folarin Kolawole

Project Administration: Christopher A. Scholz

Resources: Christopher A. Scholz Software: Shaidu N. Shaban

© 2023. The Authors. This is an open access article under the terms of the Creative Commons Attribution-NonCommercial-NoDerivs License, which permits use and distribution in any medium, provided the original work is properly cited, the use is non-commercial and no modifications or adaptations are made.

The Deep Basin and Underlying Basement Structure of the Tanganyika Rift

Shaidu N. Shaban^{1,2}, Folarin Kolawole³, and Christopher A. Scholz¹

¹Department of Earth and Environmental Sciences, Syracuse University, Syracuse, NY, USA, ²Tanzania Petroleum Development Corporation, DSM, Dar es Salaam, Tanzania, 3Department of Earth and Environmental Sciences, Columbia University, Newark, NY, USA

Abstract The oldest structures in a rift basin define incipient rift architecture, and commonly modulate the patterns of landscape evolution, sedimentation, and associated hazards in subsequent phases of rift development. However, due to deep burial beneath younger, thick syn-rift sequences, and limited resolution of seismic imaging, critical early-rift processes remain poorly understood. In the Tanganyika Rift, East Africa, we augment existing 2-dimensional (2-D) seismic reflection data with newly acquired aeromagnetic and Full-Tensor Gradiometry data to assess the deep basin and underlying basement structure. Aeromagnetic and gravity grids show a dominance of NW-trending long-wavelength (>5 km) structural fabrics corresponding to the deeper basement, and dominant NW-trending with a secondary NNE-trending shorter-wavelength (<3 km) fabric representing shallower, intra-basin structures. Seismically-constrained 2-D forward modeling of the aeromagnetic and gravity data reveals: (a) an anomalously high-density (2.35–2.45 g/cc) deep-seated, fault-bounded wedge-shaped sedimentary unit that directly overlies the pre-rift basement, likely of Mesozoic (Karoo) origin; (b) ~4 km-wide sub-vertical low-density (2.71 g/cc) structures within the 3.2 g/cc basement, interpreted to be inherited basement shear zones, (c) early-rift intra-basin faults co-located with the modeled shear zone margins, in some places defining a persistent structurally-controlled intra-basin "high," and (d) a shallow intra-sedimentary V-shaped zone of comparatively dense material (~2.2 g/cc), interpreted to be a younger axial channel complex confined between the intra-basin "high" and border fault. These results provide new insight into the earliest basin architecture of the Tanganyika Rift, controlled by inherited basement structure, and provide evidence of their persistent influence on the subsequent basin evolution.

1. Introduction

The topographic morphology of active rift basins, especially in humid climatic settings, exert important controls on the transport pathways, character, and volume of sediments deposited (Burgess et al., 1989; Gawthorpe & Leeder, 2000; Kolawole, Firkins, et al., 2021; Morley et al., 1990; Rosendahl, 1987; Scholz et al., 1990). Accordingly, deciphering the structural controls on both the basin architecture and landscape evolution in such tectonic settings is of paramount importance for understanding the evolution of the Earth as well as solving problems in the applied fields of mineral and hydrocarbon exploration, hydrogeology, hydrology, subsurface CO₂ storage, and geothermal energy (Vasuki et al., 2014). Rift structures such as border and intra-basin faults, intra-basin fault blocks, accommodation zones, and transfer faults control the spatial and temporal distribution of sedimentary facies in continental rifts (Lambiase & Bosworth, 1995; Shaban et al., 2021). Many ancient and modern rift zones host lacustrine basins (e.g., Corti et al., 2022; Katz, 1990; Rosendahl, 1987) that form robust archives of tectonic history and paleoclimate dynamics.

Rift basins are structurally complex and are typically composed of a series of asymmetric fault-bounded sub-basins (Corti et al., 2022; Lambiase, 1990; Logatchev & Zorin, 1992; Morley, 1988; Muirhead et al., 2019; Rosendahl, 1987; Scholz et al., 2020; Sherman, 1992). The evolution of rift zones involves the development of regular along-axis structural segmentation into sub-basins that are bounded by large-offset border fault systems that flip polarity along-trend (Ebinger, 1989; Laó-Dávila et al., 2015; Morley et al., 1990; Rosendahl, 1987). This along-trend segmentation of rift basins may occur at inherited pre-rift basement structures such as craton boundaries, terrane boundaries, and exhumed ductile shear zones that are rift-orthogonal or rift-oblique (e.g., Corti et al., 2007; Daly et al., 1989; Dixon et al., 1987; Katumwehe et al., 2015; Kolawole et al., 2022; Laó-Dávila et al., 2015; McConnell, 1972; Nelson et al., 1992; Versfelt & Rosendahl, 1989; Wright et al., 2020).

SHABAN ET AL. 1 of 28

19449194, 2023, 7, Downloaded from https://agupubs.onlinelibrary.wiley

.com/doi/10.1029/2022TC007726, Wiley Online Library

on [04/07/2023]. See the Terms

articles are governed by the applicable Creative Commons Licens



Supervision: Christopher A. Scholz **Validation:** Folarin Kolawole, Christopher A. Scholz

Writing – original draft: Shaidu N.

Shaban

Writing – review & editing: Shaidu N. Shaban, Folarin Kolawole, Christopher A. Scholz Inherited pre-rift basement structures are widely documented to exert prominent control on the evolution of continental rift zones. At continental scales, the tectonic break-up of continents generally occurs along ancient orogenic belts or long-lived crustal scale weakness zones (e.g., Vauchez et al., 1997; J. T. Wilson, 1966). At the basin scale, studies have used seismic reflection data (e.g., Morley, 2017; Phillips et al., 2016), seismicity data (e.g., Chisenga et al., 2023; Kolawole et al., 2018), remote sensing data (e.g., Hussein et al., 2006; Laó-Dávila et al., 2015; Muirhead et al., 2019; R. W. Wilson et al., 2010), or field geological mapping (e.g., Beacom et al., 2001; Daly et al., 1989; Dixon et al., 1987; McConnell, 1972; Morley et al., 2004; U. Ring, 1994; U. W. E. Ring et al., 2005; Smith & Mosley, 1993; Wedmore et al., 2020; Wheeler & Karson, 1989) to decipher the influence of pre-existing basement structures on the evolution of rift zones. Studies have also used high-resolution aeromagnetic data to investigate the relationships between inherited basement structures and the localization and geometry of rift faults (e.g., Katumwehe et al., 2015; Kinabo et al., 2007; Kolawole et al., 2018; Kolawole, Firkins, et al., 2021; Kolawole, Phillips, et al., 2021; Kolawole et al., 2022). However, using these various data sets in isolation often presents limitations, either in terms of spatial coverage, scale, imaging resolution, dimension (single or multi), and/or depth of investigation. Notably, a few studies have adopted the integration of Full-Tensor Gradiometry (FTG), aeromagnetic data, and seismic reflection data for the analysis of tectonic structures (e.g., Jamaludin et al., 2021; Malin, 2017; Peace et al., 2018). Although several studies have examined the evolving rift basins of the East African Rift System (EARS) (e.g., Morley, 1999; 2002), the geometry and kinematics of the earliest fault systems are still poorly constrained (Ebinger et al., 2019; Kolawole, Phillips, et al., 2021).

Here, for the first time, we investigate rift processes by integrating FTG, aeromagnetic, and 2-dimensional (2-D) seismic reflection data from a unique, biologically diverse, ecologically sensitive, resource-rich, and tectonically active rift basin, the Tanganyika Rift segment of the EARS (Figures 1a and 1b). The primary objective of this study is to better characterize the deep-to-shallow basin structure of the Lake Tanganyika Rift (LTR), and the architecture of the pre-rift crystalline basement beneath its ~2–6-km thick sedimentary fill (Figure 1b). The extended objectives include: (a) updating the previously published fault map of the basin, and (b) assessing the possible presence of Pre-Cenozoic (i.e., Permo-Triassic age "Karoo" and Cretaceous) rift sediments, and (c) studying the subsurface structure of the Kavala Island Ridge (KIR), and its relationship with the Mahale Mountains and Katenga–Kugulu–Ntengo lineaments. The KIR is the most prominent structural high in the LTR separating the modern lake into distinct limnological domains (Scholz et al., 2003), and served as a paleodrainage divide during lowstands, and separates major faunal groups (Scholz & Rosendahl, 1988).

1.1. Background

1.1.1. The East African Rift System (EARS)

The EARS runs from the Red Sea and Gulf of Aden in the north to Mozambique and Botswana in the south, with a length of ~4,000 km and width of 50–150 km (Morley, 1999; Chorowicz, 2005; Figure 1a). EARS rifting initiated in the Oligocene contemporaneously with the opening of the Red Sea and Gulf of Aden (Wolfenden et al., 2005). The EARS is composed of a series of rift segments (typically ~80–150 km long), predominantly in the form of asymmetric half-graben basins (Morley, 1989; Rosendahl, 1987) although in some sectors of the EARS (e.g., Ethiopia) rifting does not always exhibit alternating asymmetric half graben (Corti et al., 2022). The rift is comprised of two branches, the Eastern Branch and Western Branch, separated by the Archean Tanzania Craton at the terminus south of the Main Ethiopian Rift (Figure 1a) (Ebinger, 1989; Rosendahl, 1987). The Eastern Branch has a series of volcanic centers along strike spaced every ~20–100 km, and a long history of effusive magmatism. In contrast, the Western Branch is magma-poor, with a few volcanic centers including the Virunga Volcanic Province and the Rungwe Volcanic Province to the north and south of Lake Tanganyika respectively (Baker, 1971; Biggs et al., 2009; Furman, 2007; George et al., 1998; Mohr & Wood, 1976; O'Donnell et al., 2013). Currently the Western Branch has a maximum crustal stretching rate of 2.9 mm/yr, whereas the Eastern Branch is stretching at rates up to 5.2 mm/yr (Saria et al., 2014).

1.1.2. Lake Tanganyika Rift (LTR)

The LTR (Figure 1) is situated in the Western Branch, and it holds the deepest and most voluminous lake in Africa (\sim 645 km long and maximum water depth of 1,470 m) (Capart, 1952; Coulter, 1963; Rosendahl, 1987; Shaban et al., 2021). The timing of LTR initiation is not well resolved due to the lack of information from the basal basin fill. Cohen et al. (1993) suggested an initial age of \sim 9–12 Ma based upon the extrapolation ages

SHABAN ET AL. 2 of 28

19449194, 2023, 7, Downloaded from https://agupubs.onlinelibrary.wiley.com/doi/10.1029/2022TC007726, Wiley Online Library on [04/07/2023]. See the Terms and Conditions (https://onlinelibrary.wiley

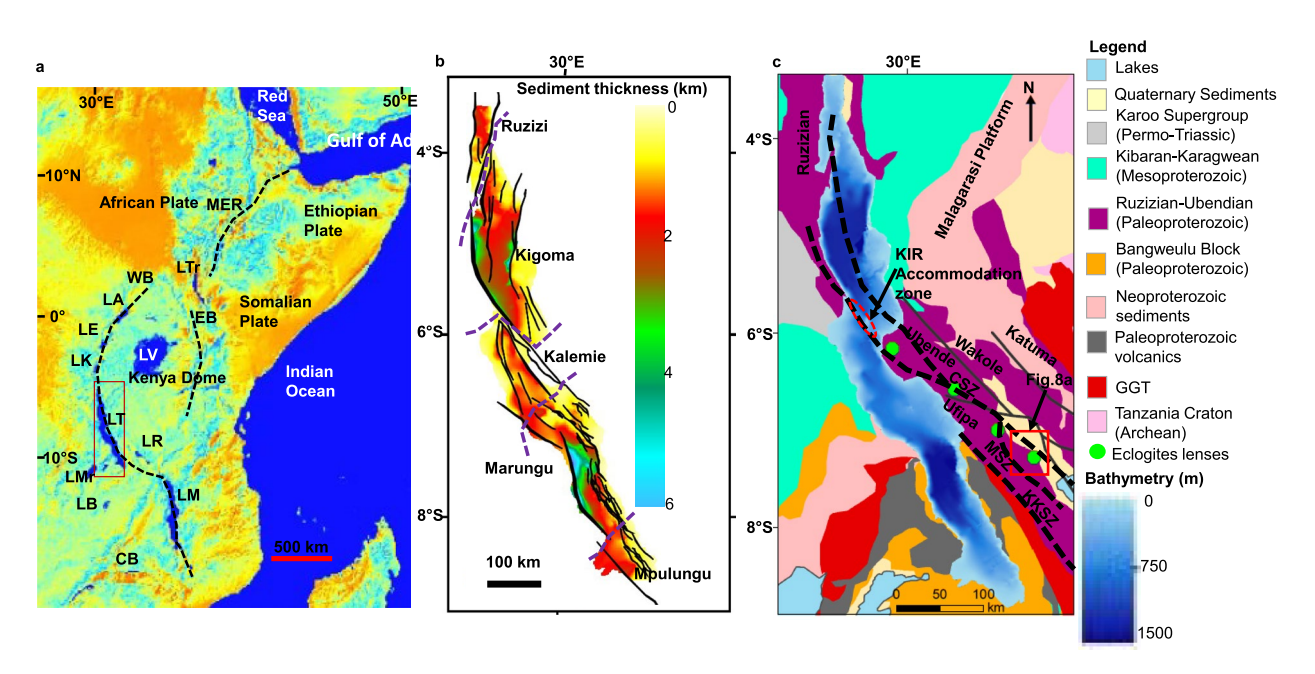


Figure 1. Study area: (a) Digital Elevation Model of the East African Rift System showing the location of Lake Tanganyika (red rectangle) along its Western Branch. WB and EB are the Western and Eastern Branches respectively. MER = Main Ethiopian Rift, LTr = Lake Turkana, LA = Lake Albert, LE = Lake Edward, LK = Lake Kivu, LT = Lake Tanganyika, LR = Lake Rukwa, LMr = Lake Mweru, LB = Lake Bangweulu, LM = Lake Malawi, and CB = Cabora Bassa dam. (b) Map of Tanganyika Rift syn-rift sedimentary thickness. Purple dashed lines show the boundary of structural provinces of the Lake Tanganyika Rift (LTR). Thick black lines show the basement-rooted normal faults (updated after Muirhead et al., 2019). Note the maximum of ~6 km thick sediments along the western border fault of the Marungu Province. (c) Geological map of the region surrounding the LTR (modified after Boniface & Tsujimori, 2021; Choubert et al., 1968); note Mesozoic rift sediments (Karoo) on the western flank of the Tanganyika Rift. Delvaux (2001) suggested the extension of Karoo sediments into the Kalemie and northern part of the Marungu provinces of the Tanganyika Rift. CSZ = Chisi Shear Zone, MSZ = Mtose Shear Zone, Kate-Kipili Shear Zone. The red rectangular polygon shows the location of Figure 8a. The red ellipse in the central part of the LTR represents a location of the Kavala Island Ridge. Bathymetry presented is derived from seismic reflection data set used in this study (maximum water depth = 1,471 m). The two major deep-water areas are in the Kigoma and Marungu provinces.

of near surface sediment cores, Pasteels et al. (1989) suggest 7.8–5 Ma, Roberts et al. (2012) suggest an age of 25–26 Ma based upon tephra ages within a nearby terrestrial rift sequence, whereas Jess et al. (2020) suggest that the age of initial rifting was coincident with the early uplift of the Ruwenzori Mountains (Eocene–Paleogene). The LTR is one of the world's largest and deepest active rift-lake systems and a site where processes of rift basin formation can be studied today. It is endowed with one of the oldest and most continuous records of tropical climate on the continents (Russell et al., 2020). The LTR is composed of a series of half grabens, typically ~80–140 km long and ~50–70 km wide (Muirhead et al., 2019; Rosendahl, 1987; Rosendahl et al., 1986; Shaban et al., 2021; Wright et al., 2020). Shaban et al. (2021) suggested three main bathymetric basins (Ruzizi, Kigoma, and Marungu-Mpulungu basins) and several sub-basins from the northern end to the southern end of the LTR (Figure 1b). These basins are bounded by nine border faults and are kinematically linked by accommodation zones partitioning extension along strike (Morley, 1988; Muirhead et al., 2019; Rosendahl, 1987; Wright et al., 2020). Depending on the rifted terrane-type (e.g., Archean vs. Proterozoic lithosphere), border faults accommodate ~90% of the extensional strain (Muirhead et al., 2019; Wright et al., 2020) with the rates of normal border fault slip increasing with the system evolution (Muirhead et al., 2019; Wright et al., 2020). The normal fault systems influence sediment pathways into the basin (Burgess et al., 1989; Rosendahl, 1987; Shaban et al., 2021).

The LTR exhibits two main directions of extension, NE-SW in the south and E-W in the northern part (Delvaux & Barth, 2010; Morley, 2010), with variable total extension (e.g., ~2.75 km in the south, 7.07–7.15 km in the central region, and ~3.75 km in the north) (Wright et al., 2020). It exhibits high topographic relief in several localities such as the Mahale Mountains, including some rift shoulder uplifts more than 1,500 m above the lake surface adjacent to border faults (Delvaux, 2001; Rosendahl, 1987; Wright et al., 2020).

The LTR is surrounded by Proterozoic and early Phanerozoic mobile belts of high-grade metamorphic rocks (Choubert et al., 1968). These geological terranes wrap around the Archean Tanzania craton to the east, and the Congo craton to the west (Figure 1c). In the north, the LTR is bounded by the NNW-SSE-striking Ubendian

SHABAN ET AL. 3 of 28

19449194, 2023, 7, Downloaded from https://agupubs.onlinelibrary.wiley.com/doi/10.1029/2022TC007726, Wiley Online Library on [04/07/2023]. See the Terms

belt (2.05-1.8 Ga) and the NE-SW-striking Kibaran belt. The Ubendian belt, an amphibolite facies ductile lateral shear belt, extends to the southeast of the rift where it intersects with the Usagaran belt and the Irumide belt (Figure 1c). It consists predominantly of NW to NNW trending Paleoproterozoic granitoids and medium to high-grade metamorphosed granitoids including gneisses (hornblende-rich mafic, biotite-bearing granitic gneisses, mylonitic garnet-kyanite gneisses, mylonitic felsic gneisses and high-pressure mafic granulites), granites, mica schists, ultramafics, and eclogites. Daly et al. (1985) and Daly (1988) divided the Ubdendian belt into eight litho-tectonic terranes from the northeast to the south: Ubende (metabasites, mafic and ultra-mafic bodies), Wakole (alumino-silicate schists), Katuma (Bt gneisses), Ufipa (gneissic granite), Mbozi (metabasic granulites, quartzites), Lupa (metavolcanics), Upangwa (meta-anorthosite), and Nyika (Cordierite gneisses) (Figure 1c). These terranes are bounded by NW-SE oriented multiphase sinistral strike-slip mylonite zones that are attributed to persistent Proterozoic wrench fault reactivation as they define the general trend of the rift faults (Boven et al., 1999; Theunissen et al., 1996). Eclogite outcrops (lenses between 1 and 100 m) have been reported in the Ubende and Ufipa terranes whereby the Ubende eclogites are mylonitic eclogites and those in the Ufipa terrane are not mylonitic but rather coarse grained and granoblastic (Sklyarov et al., 1998). Based on similar geology and geochronology, Boniface and Tsujimori (2021) grouped Ubendian terranes into three groups; the Western Corridor (Ufipa and Nyika), the Central Corridor (Ubende, Mbozi, and Upangwa), and the Eastern Corridor (Katuma and Lupa). Accordingly, because the Wakole Terrane is entirely composed of Mesoproterozoic metasedimentary rocks without any traces of Paleoproterozoic traces (Boniface et al., 2014), it was excluded from the grouping. The belt is intruded by a few carbonatites of Mesoproterozoic to Mesozoic ages. The Kibaran belt extends to the northwest of the rift and is composed of orthogneisses and high-grade metasediments, schists, quartzites, metaquartzites, and granites (Boniface & Tsujimori, 2021; Boniface et al., 2012; Fernandez-Alonso & Theunissen, 1998; Sutton et al., 1954) (Figure 1c). In the east, the LTR is bounded by the NE-SW oriented Karagwe-Ankolean Belt, the Ubendian Belt, and the NNW-SSE oriented Malagarsi Platform. The Malagrasi Platform is predominantly composed of Neoproterozoic sediments, whereas, the Kibaran and the Karagwe-Ankolean Belts are composed of arenaceous and pelitic metasediments overprinted by greenschist- to amphibolite-facies signature. The Kibaran metasediments are intruded by mafic-ultramafic layered igneous complexes together with the predominantly S-type granitic magmas (Duchesne et al., 2004; Fernandez-Alonso & Theunissen, 1998; Tack et al., 1994, 2010). Based on U-Pb zircon dating of 1,079 ± 14 Ma, the greenschist- to amphibolite-facies metamorphic imprints on the Karagwe-Ankolean Belts are a precursor to the Mesoproterozoic emplacement of tin-granitoids magmatism (Kokonyangi et al., 2006). In the southwest, the Rift is bounded by the Katanga supergroup that is mainly composed of Neoproterozoic sediments. At its southern extent, the LTR continues into the Paleoproterozoic Bangweulu cratonic Block adjacent to Karoo structures (Daly et al., 1989; Klerkx et al., 1998; Lenoir et al., 1994; Morley, 2010). It is surrounded by Proterozoic mobile orogenic belts such as the Mesoproterozoic Kibaran and Irumide Belts in the west and the Neoproterozoic Lufilian Belt in the southwest (Figure 1c). The Bangweulu Block is composed of E-W oriented schist belt (migmatitic biotite gneiss, biotite-epidote, and muscovite gneiss, mica-schist, pelitic schist, amphibolite, and recrystallized quartzite), rhyolitic tuff, basalts, granites and a volcano-plutonics complex (explosive volcanics, mafic, and felsic plutons). A large part of the basement is covered by the Paleoproterozoic Mporokoso Group metasediments (Andersen & Unrug, 1984).

Little is known about the sedimentary geology of the deepest parts of the Rift. Shallow coring of the Holocene and Upper Pleistocene sections penetrated diatomaceous ooze-rich shale, sands, siltstone, and localized carbonates (Felton et al., 2007; Livingstone, 1965; McGlue et al., 2008, 2020; Scholz et al., 2003; Tiercelin et al., 1988, 1992). The LTR contains more than ~6 km of syn-rift lacustrine sediments in some areas, as evident in 2-D seismic reflection data (Morley, 1988, Muirhead et al., 2019; Rosendahl, 1987; Shaban et al., 2021; Wright et al., 2020; Figure 1b) distributed in at least six depositional units (Figures 2b and 2c; Muirhead et al., 2019; Shaban et al., 2021). The units consist of S1 (oldest) to S6 (youngest) deposits. S2–S6 generally record deeper water rift lake sequences, manifested by the increasing dominance of the high amplitude and parallel to semi-parallel seismic reflections. S3–S5 records facies variability with higher proportion of chaotic seismic reflections and influence of alternating high- and low lake levels (Figure 2c), indicating system with increasing relief (Shaban et al., 2021).

Following the geological mapping of Choubert et al. (1968) and structural analysis of Tiercelin et al. (1988), Corti et al. (2007), and Muirhead et al. (2019), the inherited fabrics of the LTR were proposed to have two strong trends, NW-SE, and NE-SW as observed onshore in the Proterozoic metamorphic terrains that the rift transects. For instance, there is a strong NW-SE trend of pre-existing lineaments in the Ruzizian-Ubendian belts, and a localized

SHABAN ET AL. 4 of 28

19449194, 2023, 7, Downloaded from https://agupub.so.nlinelibary.witey.com/doi/10.1029/2022TC007726, Wiley Online Library on [04/07/2033]. See the Terms and Conditions (https://onlinelibrary.wiley.com/terms-and-conditions) on Wiley Online Library for rules of use; OA articles are governed by the applicable Creative Commons. Licenseauch Conditions (https://onlinelibrary.wiley.com/terms-and-conditions) on Wiley Online Library for rules of use; OA articles are governed by the applicable Creative Commons. Licenseauch Conditions (https://onlinelibrary.wiley.com/terms-and-conditions) on Wiley Online Library for rules of use; OA articles are governed by the applicable Creative Commons. Licenseauch Conditions (https://onlinelibrary.wiley.com/terms-and-conditions) on Wiley Online Library for rules of use; OA articles are governed by the applicable Creative Commons. Licenseauch Conditions (https://onlinelibrary.wiley.com/terms-and-conditions) on Wiley Online Library for rules of use; OA articles are governed by the applicable Creative Commons. Licenseauch Conditions (https://onlinelibrary.wiley.com/terms-and-conditions) on Wiley Online Library for rules of use; OA articles are governed by the applicable Creative Commons. Licenseauch Conditions (https://onlinelibrary.wiley.com/terms-and-conditions) on Wiley Online Library for rules of use; OA articles are governed by the applicable Creative Commons.

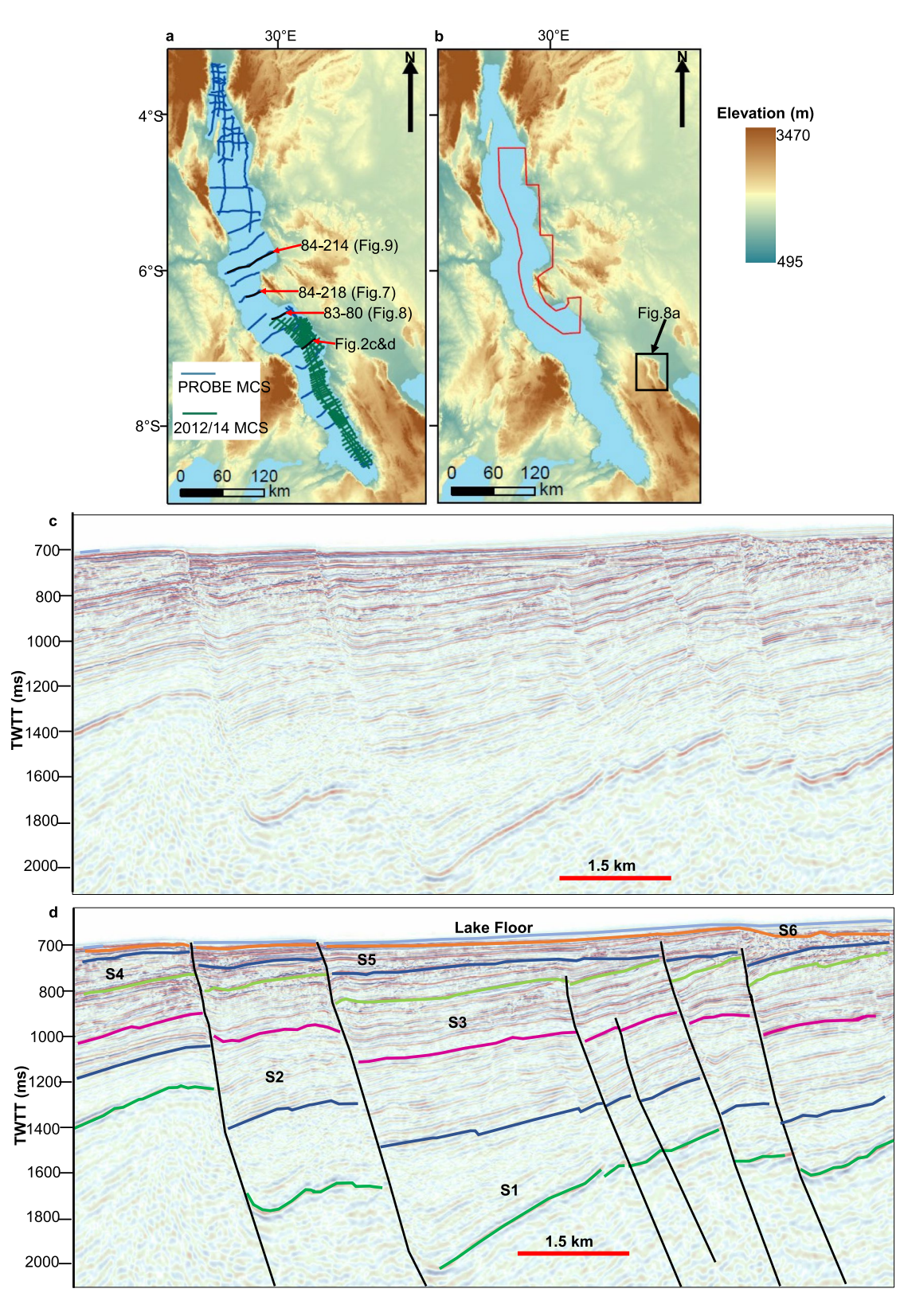


Figure 2.

SHABAN ET AL. 5 of 28

19449194, 2023, 7, Downloaded from https://agupubs.onlinelibrary.wiley.com/doi/10.1029/2022TC007726, Wiley Online Library on [04/07/2023]. See the Terms

and-conditions) on Wiley Online Library for rules of use; OA articles are governed by the applicable Creative Commons Licens

bimodal trend, NE-SW and NW-SE in the Bangweulu cratonic terrain (Figure 2). These pre-existing fabrics correlate well with the orientation of major shear structures that bound basement subterranes (e.g., Andersen & Unrug, 1984; Daly, 1988; Daly et al., 1989; Muirhead et al., 2019; Wright et al., 2020).

2. Data

2.1. Aeromagnetic Data

The aeromagnetic data were collected in 2015–2016 alongside the Tanganyika Air-FTG® survey data over the east central part of the LTR (Figure 2b) using a magnetometer system that is comprised of an airborne magnetometer and a base station. The total field was measured using the Geometrics 882 cesium vapor sensor mounted in a boom attached to the aircraft tail. The data were recorded at 10 Hz and compensated in real time by an RMS DAARC500 data acquisition system. To monitor diurnal variations in the background field, a GEM Systems GSM19 gradiometer base station was used, recording at 1 s intervals. This was backed up by a Geometrics G856 (proton precession magnetometer) base station recording at 10 s intervals. The aircraft was flown in the survey line headings (090°), and because at tropical latitudes the sensor's sensitivity weakens during turns, the figure of merit was split into partial calibrations.

The aeromagnetic data were processed by Bell Geospace Limited using Geosoft Oasis Montaj software to obtain the final measured residual magnetic intensity (RMI). Initial processing employed manual filtering to remove the interference noise from nearby artificial magnetic sources such as electrical equipment. Also, the Earth's regional magnetic field was removed from the survey data to separate local anomalies. The International Geomagnetic Reference Field (IGRF) tables corresponding to the time, date and acquisition height of the survey were generated. Then, the calculated IGRF was subtracted from the recorded total magnetic intensity (TMI) and the statistical IGRF mean for the entire survey was added back in. Alken et al. (2021) defines the IGRF as a set of spherical harmonic coefficients that are used in a mathematical model to account for the large-scale, time-varying portion of Earth's internal magnetic field between epochs 1900 A.D. Other processing of the data included leveling (tie-line and micro) and de-meaning.

Aeromagnetic signals detect subsurface geology that contains sufficient magnetic susceptibility to be magnetized by the passing of a magnetic sensor proximal to it. Therefore, high magnetic anomalies result from geology that is dominantly composed of minerals with magnetic affinities such as typically found in igneous and metamorphic rocks (crystalline basement). Consequently, the edges of sedimentary basins exhibit higher magnetic anomalies compared to the basins' axes due to their proximity to the basement rocks (Florio, 2018). Likewise, the vertical juxtaposition of basement rocks against sedimentary sequences along dip-slip faults creates prominent gradients in the aeromagnetic data (e.g., Grauch & Hudson, 2011; Kolawole et al., 2018). Accordingly, we used aeromagnetic data mainly to discern basement-rooted structures.

2.2. Airborne-Full Tensor Gradiometry (Air-FTG®) Data

The Air-FTG® data were acquired over the east central part of the LTR (Figure 2b) alongside the aeromagnetic data (refer to Section 2.1) using an FTG-1 unit owned by Bell Geospace Limited. The FTG system is comprised of three gravity gradient instruments (GGIs) mounted on a stabilized platform. The data were initially acquired in an internal coordinate system referenced to the axes of the three GGIs, which are the primary measurement components of the FTG. These data were later transformed into an East-North-Down (x, y, z) coordinate system with x and y in the plane of the Earth's surface and z perpendicular to that plane downward toward the Earth. A total of 24,027-line kilometers of Air-FTG® data with 500 m in line spacing were acquired continuously throughout a flight at a ground speed of \sim 215 km/hr over the period of 18 November 2015–20 January 2016. The tie-lines were also acquired at 5,000 m intervals at 090° heading. A drape ranged between 929 and 1,875 m above sea level

Figure 2. (a) Locations of seismic data used in this study. The latest 2D seismic data tracklines are the 2014/2014 Multi-channel Seismic Survey (MCS), the 1983/1984 data tracklines are PROBE MCS. Note the profiles (in black color) for panel (c, d), Figures 7–9. (b) The red polygon represents the Full-Tensor Gradiometry and Aeromagnetic survey area. The black rectangular polygon shows the location of Figure 8a (c, d). Example basin-scale seismic reflection NE-SW dip profile (2014), located south of the Kalya Platform in Lake Tanganyika Rift consisting of the uninterpreted (panel c) and interpreted (panel d) sections. The seismic images show six known seismic stratigraphic syn-rift units (S1, oldest, to S6, youngest). S2–S6 generally records deeper rift lake sequences, manifested by increasing the dominance of the high amplitude and parallel to semi-parallel reflections. S3–S5 records facies variability with higher proportion of chaotic reflections and influence of alternating high- and low lake levels (see also Shaban et al., 2021).

SHABAN ET AL. 6 of 28

19449194, 2023, 7, Downloaded from https://agupubs.onlinelibrary.wiley.com/doi/10.1029/2022TC007726,

Wiley Online Library on [04/07/2023]. See the Terms

of use; OA articles are governed by the applicable Creative Commons

depending on the topography. Draping the survey is the process of projecting a flight height to a safer flyable constant terrain clearance, rather than at a constant elevation above sea level to optimize the survey pilots' flight path (Evjen, 1936; Pilkington & Roest, 1992). It improves the data fit at line intersections and reduces spurious variations in signal strength between survey lines.

The data were subjected to a series of processing steps to obtain the final measured gravity gradients used for interpretation. Specific processing methods included high-rate post-mission compensation (HRPMC), strip-average-reformat (SAR), bias and drift corrections, tie-line leveling, tensor components generation, full-tensor noise reduction (FTNR) and finally, terrain corrections. The processing was done by Bell Geospace Limited.

FTG measures the derivative of all the three gravity components in all three directions (Gx, Gy, and Gz) (Figure S2 in Supporting Information S1), and enables the delineation of geology and geological structures (Dickinson et al., 2010). Conventional gravity measures only the changes in the Gz direction (i.e., the vertical component) whereas FTG enables measurement and detection of those changes in all directions (i.e., the vertical and two horizontal components). For a full swing, FTG assesses how each of the three components of the gravity vector varies in each of the three primary directions. This results in nine-component tensors (Figure S2 in Supporting Information S1). FTG can accurately measure the edges of anomaly sources and define their size, shape, and thickness. FTG data record short wavelength signals generated by shallow to intermediate sources located within 10 km below the surface (Stuckless, 2008). These signals are not recorded in conventional gravity data, hence FTG exhibits greater resolution (Stuckless, 2008).

2.3. 2-D Seismic Reflection Data

This study augments the legacy Project PROBE 2-D seismic reflection data (PROBE) acquired in 1983–1984 and reprocessed in 2016 by ION Geophysical Company. The PROBE multichannel, basin-scale seismic (MCS) data are 24-fold, widely spaced (up to ~28 km), but cover ~1,900 line-km over the entire lake and image up to 6 km below the earth's surface. Its acquisition program employed a 140 cubic inch single air gun and a 48-channel hydrophone streamer, with offsets up to 1,450 m (e.g., Burgess et al., 1989; Muirhead et al., 2019; Rosendahl, 1987; Shaban et al., 2021; Wright et al., 2020). Reprocessing details are contained in Supporting Information S1. We integrated the legacy data with state-of-the art commercial data acquired in 2012 and 2014 in the southern part of the lake within the Tanzania territory. The 2012/2014 data were acquired using a 3 km-long streamer and a 500 cubic inch air gun array and are 60-fold with a frequency range of ~5–75 Hz and a vertical resolution of 8–10 m.

3. Materials and Methods

To investigate the deep-to-shallow structure of the central LTR (4.5°S-7.5°S and 29°E-31°E), we integrate aeromagnetic and FTG anomaly derivatives, the 2-D seismic reflection data, and a digital elevation model (DEM). Our fault mapping approach follows standard practice, consistent with previous studies (e.g., Muirhead et al., 2019), albeit in the current study we augment Air-FTG® and aeromagnetic data to improve the lineament delineation, and we mostly focus on the central part of the Rift (Kigoma, Kalemie, and northern Marungu provinces) (Figures 1 and 2). The integration of FTG, magnetic data and seismic reflection data has proven to be an effective tool for structural mapping and delineating the size, shape, and thickness of target bodies in hydrocarbon exploration operations (Jackson et al., 2013; Jamaludin et al., 2021). Gravity anomalies are a function of density of the subsurface geology, thus, can be used to discriminate lithological bodies and gradients associated with faulting of those bodies.

3.1. Seismic Interpretation

We use seismic stratigraphic units (Figure 2) of Muirhead et al. (2019) and Shaban et al. (2021) as stratigraphic markers to evaluate the structural characteristics. Using DecisonSpaceTM Landmark software, we mapped major faults and minor faults respectively in the eastern-central part of the rift. We use the maps of stratigraphic markers (Nyanja Event and S3) offset by faults to discern the fault geometry. Fault mapping was augmented with the coherence seismic attribute extraction that reveals discontinuities (Figure S1 in Supporting Information S1). We

SHABAN ET AL. 7 of 28

9449194, 2023, 7, Downloaded from https

agupubs.onlinelibrary.wiley.com/doi/10.1029/2022TC007726,

Wiley Online Library on [04/07/2023]. See the Terms

on Wiley Online Library for rules of use; OA articles are governed by the applicable Creative Commons License

project offsets on the seismic unit boundaries as fault heaves. We judge fault extents based on faults with the same strike on the adjacent seismic profiles, otherwise, in case of widely spaced profiles, we assume the fault extents terminate at the midpoint of two adjacent seismic profiles. The identification of fault extent in the strike direction also depends on the scale of the observation (Gillespie et al., 1992). Thus, one fault trace on a map may be a combination of several trace segments when observed on a larger scale map (Lonergan et al., 1998). Also, the depth resolution limit of the acquisition method influences fault interpretation on seismic data sets inferred from displacement (Sheriff, 1977). We examine the fault orientations using rose diagram plots.

3.2. Aeromagnetic Data Analysis

3.2.1. Reduction of Aeromagnetic Data to the Pole

In the low magnetic latitudes, the shape of magnetic anomalies due to deep-seated vertical bodies undergoes distortion because of inclination and declination angles of the geomagnetic field. Consequently, it becomes cumbersome to correlate the observed magnetic anomalies and the positions of causative bodies (Baranov, 1957). To overcome this effect, the magnetic data are transformed as it would be measured at the magnetic poles by applying a reduction to pole (RTP) transformation (Baranov, 1957). When the magnetic survey area is located within magnetic latitude with an inclination angle less than 15° , the RTP fails to locate the anomalies exactly above the source bodies, hence, a reduction to the Equator (RTE) transformation is needed (Mono et al., 2018). Because our study area survey area is located within magnetic latitudes with magnetic inclination angle of between -20° and -40° below the Equator, to correctly locate the anomalies over the source, the TMI was reduced to the Pole (RTP) as shown in Figure 3.

3.2.2. Horizontal Gradient, Vertical Gradient, and Bandpass Filter

To aid structural mapping, subtle aeromagnetic and gravity anomalies can be better resolved using the mathematical derivatives of the TMI and gravity data such as the vertical and total horizontal derivatives (Miller & Singh, 1994; Salem et al., 2008). In the case of aeromagnetic grid filtering, the total horizontal derivative resolves the rate of change of TMI in the horizontal directions. Similarly, the vertical derivative resolves the rate of change of TMI in the vertical direction. These derivatives generally resolve structures at shallow crustal depths (high wavenumber components of the data).

However, to resolve structures at intermediate and deeper crustal depths, we apply low-pass and high-pass filters on the RTP aeromagnetic grid. For this purpose, we adopted the Butterworth bandpass filter, which has the advantage of allowing the user to specify the desired mid-range wavelengths while attenuating the low and high extremes of the wavelength continuum (Butterworth, 1930). We applied a Butterworth bandpass filter of 5–12 km to resolve shallower (intra-sedimentary) structures, 12–45 km to resolve intermediate-depth (shallow basement) structures, and 45–205 km to resolve deeper intra-basement structures (Figure 4). A rule of thumb is that ca. one-third to one-quarter of the anomaly width is an estimate to the depth of the anomaly source. The structures were extracted manually by carefully tracing the lineaments. Furthermore, we used other derivatives such as tilt derivative, analytical signals and first horizontal derivative of the vertical derivative of the aeromagnetic data to delineate lineaments (refer to the Supporting Information S1).

3.3. FTG Data Analysis

We analyzed six tensor components of FTG data to delineate geological bodies and structures. The T_{zz} directly delineates the subsurface geology revealing major sub-basins and structures, and T_{xz} delineates the axes of major structures in the north-south and east-west directions respectively, whereas T_{xx} and T_{yy} outline the edges of structures in the east-west and north-south directions.

3.3.1. Rotational Invariants

FTG invariants are effective for resolving complex subsurface structural trends in the upper crust (Mataragio & Kieley, 2009). The rotational invariants are powerful tools for identifying the density contrast between different geological features as well as visualizing all six tensor components from a single image (Mataragio & Kieley, 2009). These data sets commonly resolve high-frequency and short wavelength anomalies, corresponding to intra-sedimentary structures in basins. We use FTNR and filtered tensor data to compute rotational invariants. To remove non-geological high frequency signals, we applied a low-pass filter of 500 m to the FTNR data.

SHABAN ET AL. 8 of 28

19449194, 2023, 7, Downloaded from https://agupubs.onlinelibrary.wiley.com/doi/10.1029/202TC007726, Wiley Online Library on [04/07/2023]. See the Terms and Conditions (https://onlinelibrary.wiley.com/terms-and-conditions) on Wiley Online Library for rules of use; OA articles are governed by the applicable Creative and Conditions (https://onlinelibrary.wiley.com/terms-and-conditions) on Wiley Online Library for rules of use; OA articles are governed by the applicable Creative and Conditions (https://onlinelibrary.wiley.com/terms-and-conditions) on Wiley Online Library for rules of use; OA articles are governed by the applicable Creative and Conditions (https://onlinelibrary.wiley.com/terms-and-conditions) on Wiley Online Library for rules of use; OA articles are governed by the applicable Creative and Conditions (https://onlinelibrary.wiley.com/terms-and-conditions) on Wiley Online Library for rules of use; OA articles are governed by the applicable Creative and Conditions (https://onlinelibrary.wiley.com/terms-and-conditions) on Wiley Online Library for rules of use; OA articles are governed by the applicable Creative and Conditions (https://onlinelibrary.wiley.com/terms-and-conditions) on Wiley Online Library for rules of use o

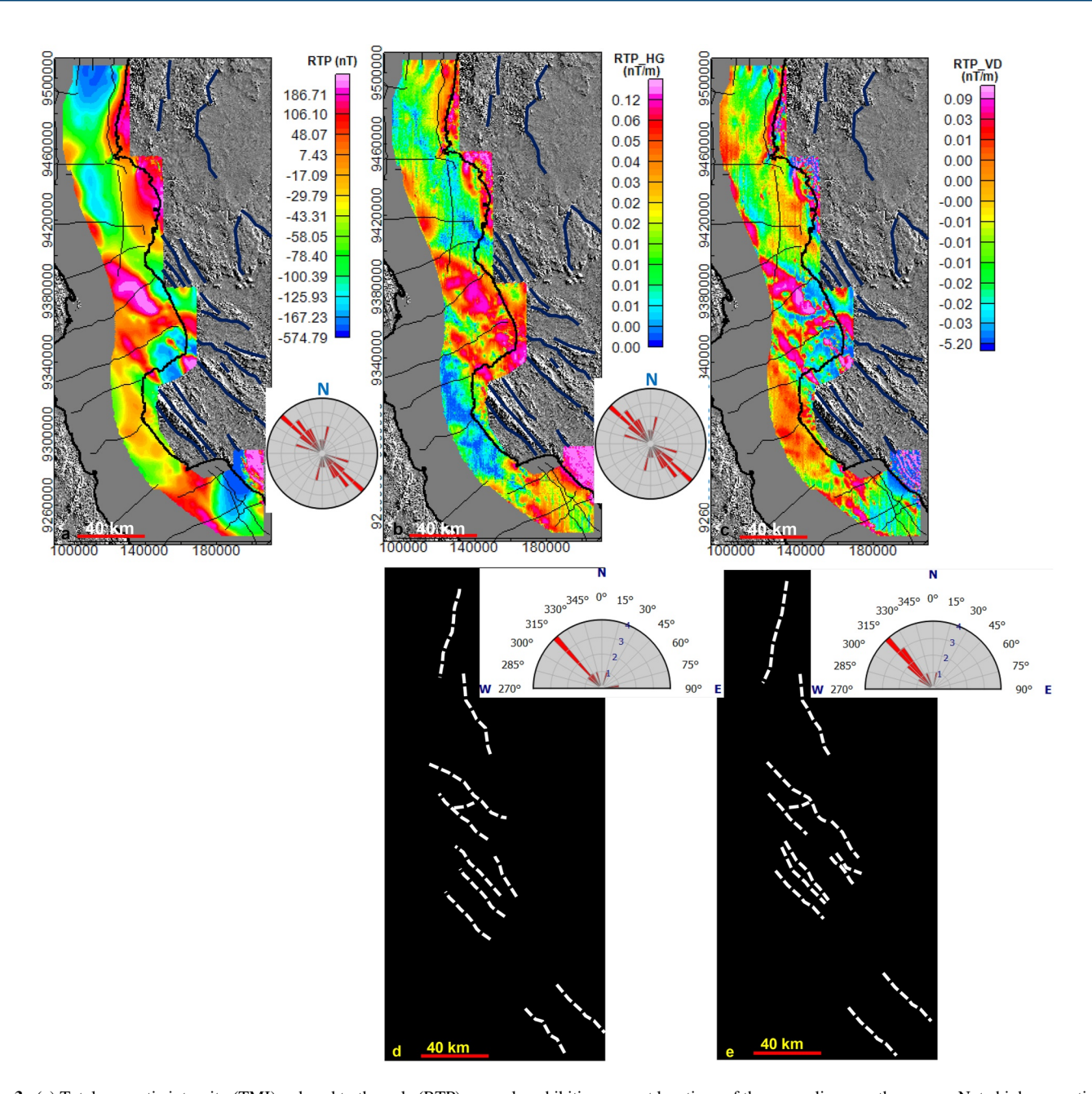


Figure 3. (a) Total magnetic intensity (TMI) reduced to the pole (RTP) anomaly exhibiting correct locations of the anomalies over the source. Note high magnetic anomaly in the southern part of the survey area (North Marungu Province) and low magnetic anomaly in the northern part of the survey area (North Kigoma Province). (b) Total Horizontal derivative (HG) of the RTP TMI anomaly. (c) Vertical derivative (Dz) of the RTP TMI anomaly. The basemap is a hillshade map created from the 30-m resolution SRTM-DEM using a sun angle of 45° and azimuth of 315° to highlight the lineaments in the study area. (d) Structures extracted from (b). (e) structures extracted from (c). The rose diagrams were created by measuring the general strike of each lineament then plotted using GeoRose software (Yong Technology Inc., 2014).

$$R-1 = \sqrt{\left((T_{xx}T_{yy} + T_{yy}T_{zz} + T_{xx}T_{zz}) - \left(T_{xy}^2 + T_{yz}^2 + T_{zx}^2 \right) \right)}$$
 (1)

$$R-2 = (T_{xx}(T_{yy}T_{zz} - T_{yz}^2)) + T_{xy}(T_{yz}T_{xz} - T_{xy}T_{zz}) + (T_{xz}(T_{xy}T_{yz} - T_{xz}T_{yy}))^{1/3}$$
(2)

The advantage of the rotational invariants (Figure 5) is the ability to retain the shape and orientation regardless of the rotation direction of the tensors about the z-axis (Mataragio & Kieley, 2009). The structures were extracted manually by carefully tracing the lineaments.

SHABAN ET AL. 9 of 28

19449194, 2023, 7, Downloaded from https://agupubs.onlinelibrary.wiley.com/doi/10.1029/2022TC007726, Wiley Online Library on [04/07/2023]. See the Terms and Conditions (https://online

governed by the applicable Creative Commons Licens



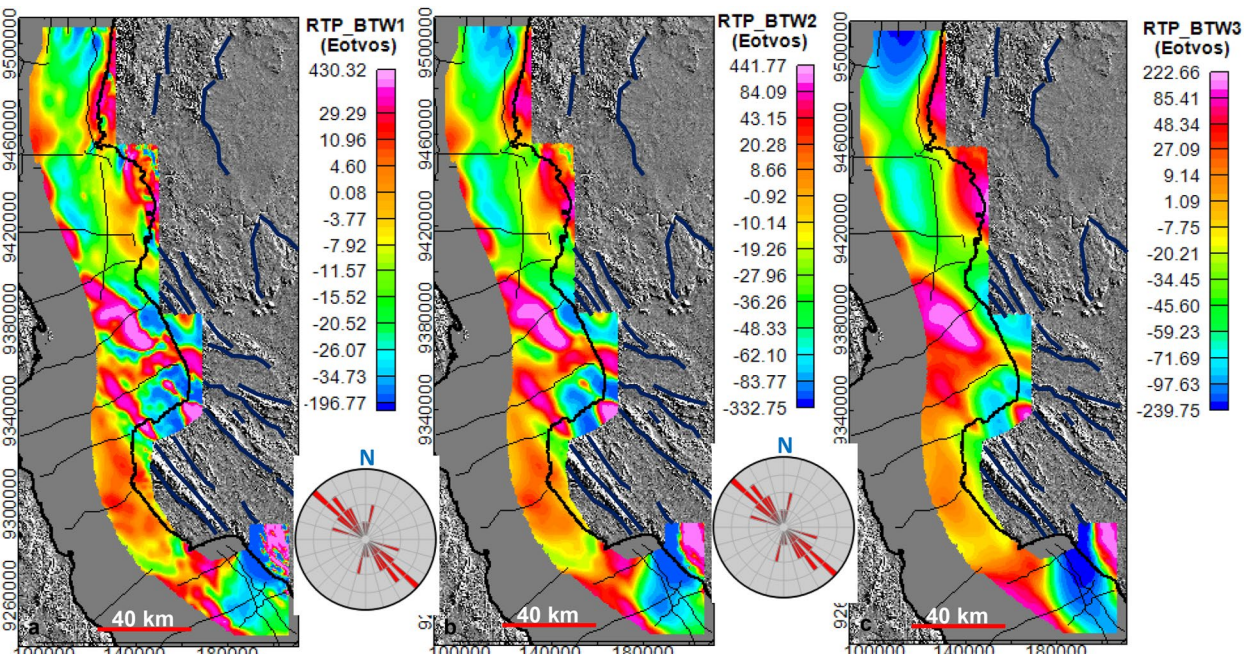


Figure 4. Butterworth bandpass filtered total magnetic intensity RTP. (a) Short wavelength, 5-12 km, (b) intermediate wavelength, 12-45 km, and (c) long wavelength, 45–205 km. The short wavelength reveals the magnetic bodies less than 2 km below the surface, the intermediate wavelength reveals magnetic bodies 2–6 km below the surface, and the long wavelength reveals magnetic bodies 6-14 km below the surface. The basemap is a hillshade map created from the 30-m resolution SRTM-DEM using a sun angle of 45° and azimuth of 315° to highlight the lineaments in the study area.

3.3.2. Upward Continuation

The observed Bouguer gravity anomaly is a sum of the regional and residual fields (Mickus et al., 1991). Thus, at any observation point, the gravity anomaly is a total of anomalies from large, deep-seated source bodies and small, localized source bodies close to the observation point. Thus, as a secondary approach for evaluating the relationship between shallow and deep basement structures, we separated the regional and residual field by upward continuation of the gravity data set. This operation shifts the data by a constant height level above the Earth's surface (Jacobsen, 1987). According to Jacobsen (1987), if a potential field is upward continued to a height z, then sources situated at a depth greater than 0.5z can be imaged. Based on the 2D seismic data the crystalline basement in the LTR is perceived within 5-6 km (Muirhead et al., 2019; Rosendahl, 1987; Shaban et al., 2021; Wright et al., 2020); therefore, to remove the short wavelength anomalies corresponding to intra-sedimentary depth intervals, the data was upward-continued at 12 km. Furthermore, we used other derivatives such as adaptive tilt angle (ATA) and tilt derivative horizontal derivative (TDX) from the FTG anomaly (T_{\cdot}) data to delineate lineaments (refer to the Supporting Information S1).

3.4. 2.75-D Gravity and Magnetic Forward Modeling

To test the possible presence of Karoo sediments within the LTR, we modeled three NW-SE profiles that run parallel to PROBE seismic profiles 84-216 (south of the KIR), 84-214 (across the KIR) and 83-80 (northern parts of the Marungu Province) (Figure 2a). Profiles were chosen to pass through the areas where Karoo sedimentary rocks were previously interpreted (Delvaux, 2001) except 84-214 was chosen to test the presence of ultramafic rocks in the subsurface. 2.75-D modeling assumes a length of target (y-dimension) has a variable strike length in each of +y and -y direction. We assumed a general increase of density with increase of depth from the lake floor. We augmented this assumption with known densities from the shallow coring within the rift (e.g., Scholz et al., 2003) and analogs from the Malawi rift (e.g., Scholz et al., 2006). In deeper intervals where there is no possible analog, so we used Gardner's equation (Equation 3) to predict lithological densities.

$$\rho = 0.31v^{0.25} \tag{3}$$

SHABAN ET AL. 10 of 28

19449194, 2023, 7, Downloaded from https://agupubs.onlinelibary.witey.com/doi/10.1029/2022TC007726, Wiley Online Library on [04/07/2023]. See the Terms and Conditions (https://onlinelibary.witey.com/terms-and-conditions) on Wiley Online Library for rules of use; OA articles are governed by the applicable Cerative Commons. License and Conditions (https://onlinelibary.witey.com/terms-and-conditions) on Wiley Online Library for rules of use; OA articles are governed by the applicable Cerative Commons. License and Conditions (https://onlinelibary.witey.com/terms-and-conditions) on Wiley Online Library for rules of use; OA articles are governed by the applicable Cerative Commons. License and Conditions (https://onlinelibary.witey.com/terms-and-conditions) on Wiley Online Library for rules of use; OA articles are governed by the applicable Cerative Commons. License and Conditions (https://onlinelibary.witey.com/terms-and-conditions) on Wiley Online Library for rules of use; OA articles are governed by the applicable Cerative Commons. License and Conditions (https://onlinelibary.witey.com/terms-and-conditions) on Wiley Online Library for rules of use; OA articles are governed by the applicable Cerative Commons. License and Conditions (https://onlinelibary.witey.com/terms-and-conditions) on Wiley Online Library for rules of use; OA articles are governed by the applicable Cerative Commons.

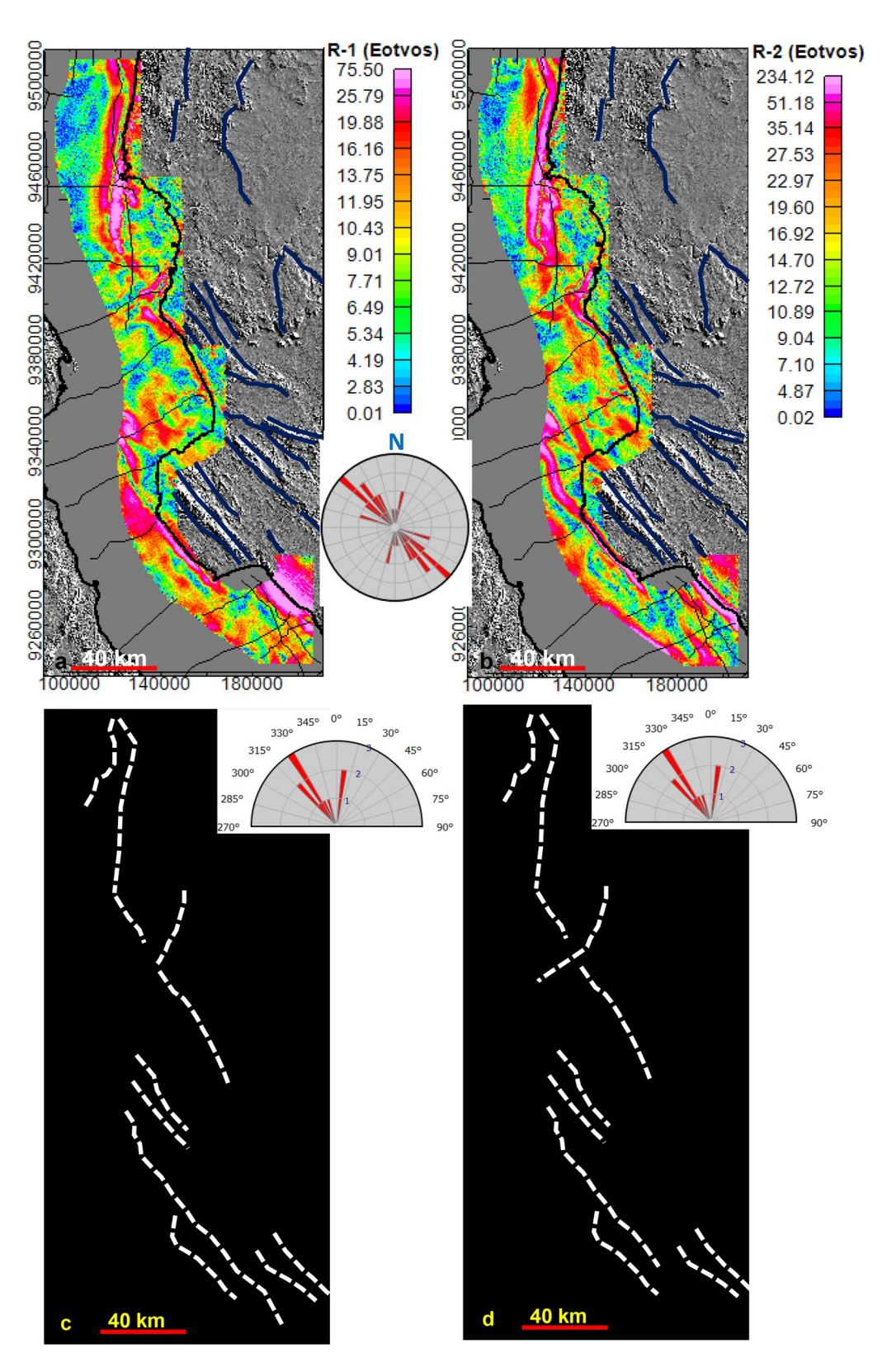


Figure 5.

SHABAN ET AL. 11 of 28

19449194, 2023, 7, Downloaded from https://agupubs.onlinelibrary.wiley.com/doi/10.1029/2022TC007726, Wiley Online Library on [04/07/2023]. See the Terms

and Conditions (https://onlinelibrary.wiley

governed by the applicable Creative Commons Licens

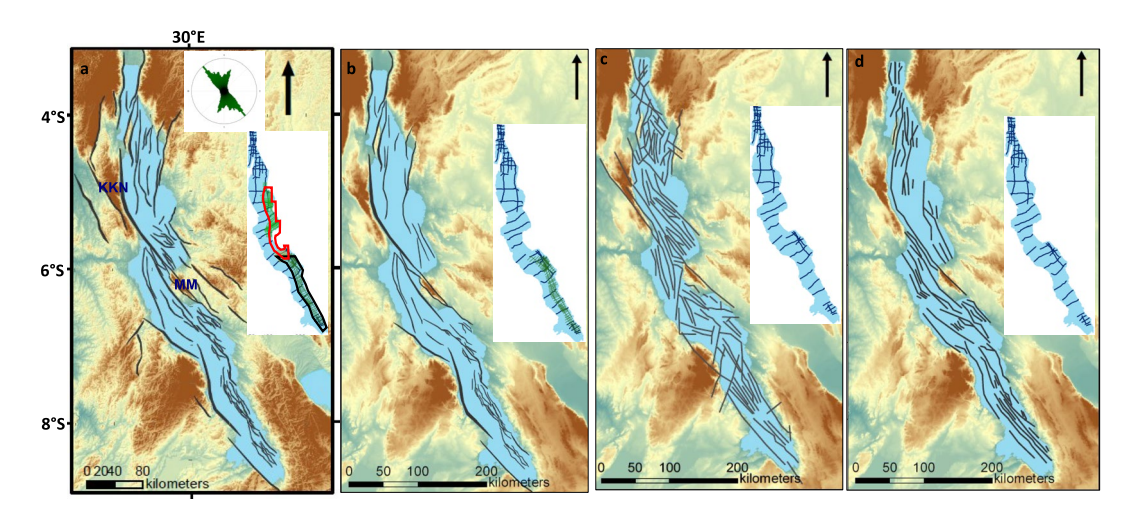


Figure 6. (a) Updated fault map of the Lake Tanganyika Rift from this study. MM and KKN represent the Mahale Mountains and Katenga–Kugulu–Ntengo lineaments respectively. The rose diagram shows the strikes of the mapped faults. Note that many faults mapped on the eastern part of the northern and central Lake Tanganyika are due to denser data coverage. (b–d) Previously published fault maps from Muirhead et al. (2019) in panel (b), Rosendahl et al. (1992) in panel (c), and Morley (1988) in panel (d). Note that our study has identified more faults within Lake Tanganyika and identified some NNE-SSW secondary fault trends in addition to the dominant NW-SE fault trend. Other structural strikes are NNW-SSE, NNE-SSW, and N-S. The inset map shows the data used during each study. The red and black polygons on panel (a) inset map demarcate the areas with Air Full-Tensor Gradiometry data, and the lines represent various 2D seismic profiles (refer to Figure 1).

where ρ = predicted density, ν = velocity obtained from seismic reflection data. We acknowledge however that the velocity information obtained from seismic data has inherent uncertainties, which we address the seismic processing section in Supporting Information S1.

4. Results

4.1. Rift Structures

The interpretation and integration of 2-D seismic reflection data, FTG, and aeromagnetic data reveal both shallow and deep structures along the LTR.

4.1.1. Shallow Structural Fabrics

The total horizontal derivative, vertical derivative (Figures 3a–3c), analytical signal, and tilt-angle derivative (Figures S3a–S3b in Supporting Information S1) reveal structures with a general dominant trend of NW-SE (Figures 3d–3f). However, we note that the tilt-angle derivative, which normalizes anomalies, resolves a secondary NE-SW trend (Figure S3 in Supporting Information S1). These derivatives generally reveal shallow upper crustal structures. Most of the resolved structures are within the south-eastern part of the Kigoma Province and the northern part of the Marungu Province (Figures 3, 5, and 6, Figure S3 in Supporting Information S1). In the southern part of the Kigoma Province, the horizontal gradient reveals lineaments of alternating magnetic polarities, with dominantly NW-SE trends.

The Butterworth filter for short wavelength anomalies in the aeromagnetic data (Figure 4a) also shows a dominance of NW-trending lineaments along the rift, with a prominent NE-trending lineament in the Kigoma Sub-basin, at the same location where the tilt-angle derivative shows NE-trending lineaments. The rotational invariants of the FTG data (Figures 5a and 5b) reveal high frequency lineaments along the rift basin, showing a dominance of a NW-SE (~315°) trend, with a prominent secondary NNE-SSW (20°) trend (Figures 5c and 5d). The maps show that the NNE-SSW lineaments dominantly occur in the northern sub-basins of the rift

Figure 5. Rotational invariants anomaly showing high-to-medium frequency and short-to-intermediate wavelength anomaly lineaments (corresponding to shallow and intermediate depth intervals). (a) R-1 and (b) R-2, showing contacts, edges, and shapes of high-density geological bodies. Note NW-striking bodies (314° mean trend) in the central and southern parts and NNE-striking bodies (009° mean trend) in the northern part of the area. (c, d) Structural fabrics mapped in panels (a) and (b) respectively. The basemap is a hillshade map created from the 30-m resolution SRTM-DEM using a sun angle of 45° and azimuth of 315° to highlight the lineaments in the study area.

SHABAN ET AL. 12 of 28

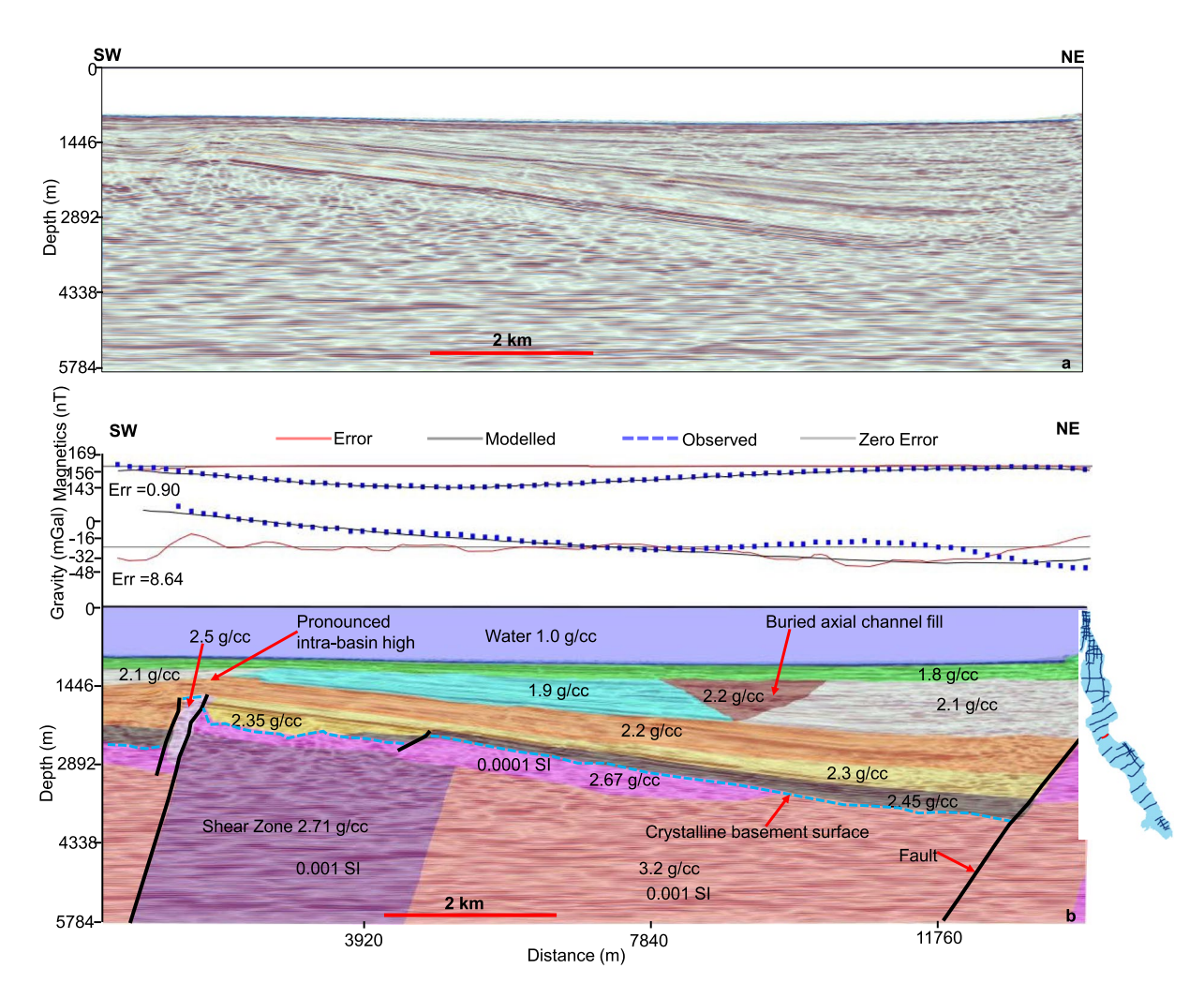


Figure 7. (a) NE-SW PROBE seismic profile 218 (see red line transect in the side-inset map in (b) and in Figure 2) located in the Central Tanganyika Rift (Kalemie Sub-basin). (b) Forward model of the Gravity (T_z) and Magnetic (residual magnetic intensity) along the seismic profile 218. Modeled geology: each colored polygon represents a block of distinct density and magnetic susceptibility from its neighboring block. Note the high density (3.2 g/cc) basement and lower-density (2.71 g/cc) intra-basement shear zone along the margins of which a large intra-basinal fault localized. The forward model permits both subvertical and moderate dip for the modeled shear zone. Thus, the down-dip alignment of the fault and shear zone is strictly aesthetic. In the sedimentary sections, the seismic shows a persistent intra-basin "high" controlled by the footwall of the intra-basin fault. Also, the model suggests the possible presence of deep-seated high-density sedimentary rocks (2.45 g/cc), likely representing Mesozoic (Karoo) rift phase units. Note the channel complex (2.2 g/cc) within the younger sedimentary intervals (seismic units 3–4 in Shaban et al., 2021).

(Kigoma/Ruzizi Sub-basins). Overall, these inferred shallow lineaments, all dominantly trending NW-SE, are consistent with the regional trends of basement lineaments on the neighboring rift shoulder (see SRTM DEM hillshade map in Figures 6 and 8, Figure S5 in Supporting Information S1).

To better discern magnetic bodies, we compared RTP TMI to its AS, because the AS produces a positive anomaly for magnetic sources only. The AS exhibits high positive anomaly lineaments mostly in the central area and a few in the northern parts of the rift (Figures S3a and S3b in Supporting Information S1). Moderate positive anomalies occur in the northern part of the Marungu Province. When compared with the T_z data, the opposite is observed; the southern part of the survey (northern part of the Marungu Province) is marked by very low gravity anomalies. High gravity anomalies are observed at the KIR, northeast of the KIR and around the Karema/Ikola Platform (Figures S6a and S6b in Supporting Information S1). Within the Mahale-KIR–Katenga–Kugulu–Ntengo corridor, the bandpass filtered RTP maps reveal ~E-W oriented lineaments with very high amplitudes (Figures 4a and 4b).

4.1.2. Deeper Structural Fabrics

High magnetic anomalies (>250 nT) in the intermediate- and long-wavelength Butterworth filtered-maps dominate the central and southern parts of the Tanganyika Rift and they dominantly trend NW-SE (Figures 4a–4c).

SHABAN ET AL. 13 of 28

19449194, 2023, 7, Downloaded from https://agupubs.onlinelibrary.wiley.com/doi/10.1029/2022TC007726, Wiley Online Library on [04/07/2023]. See the Terms and Conditions (https://onlinelibrary.wiley.com/rems-and-conditions) on Wiley Online Library for rules of use; OA

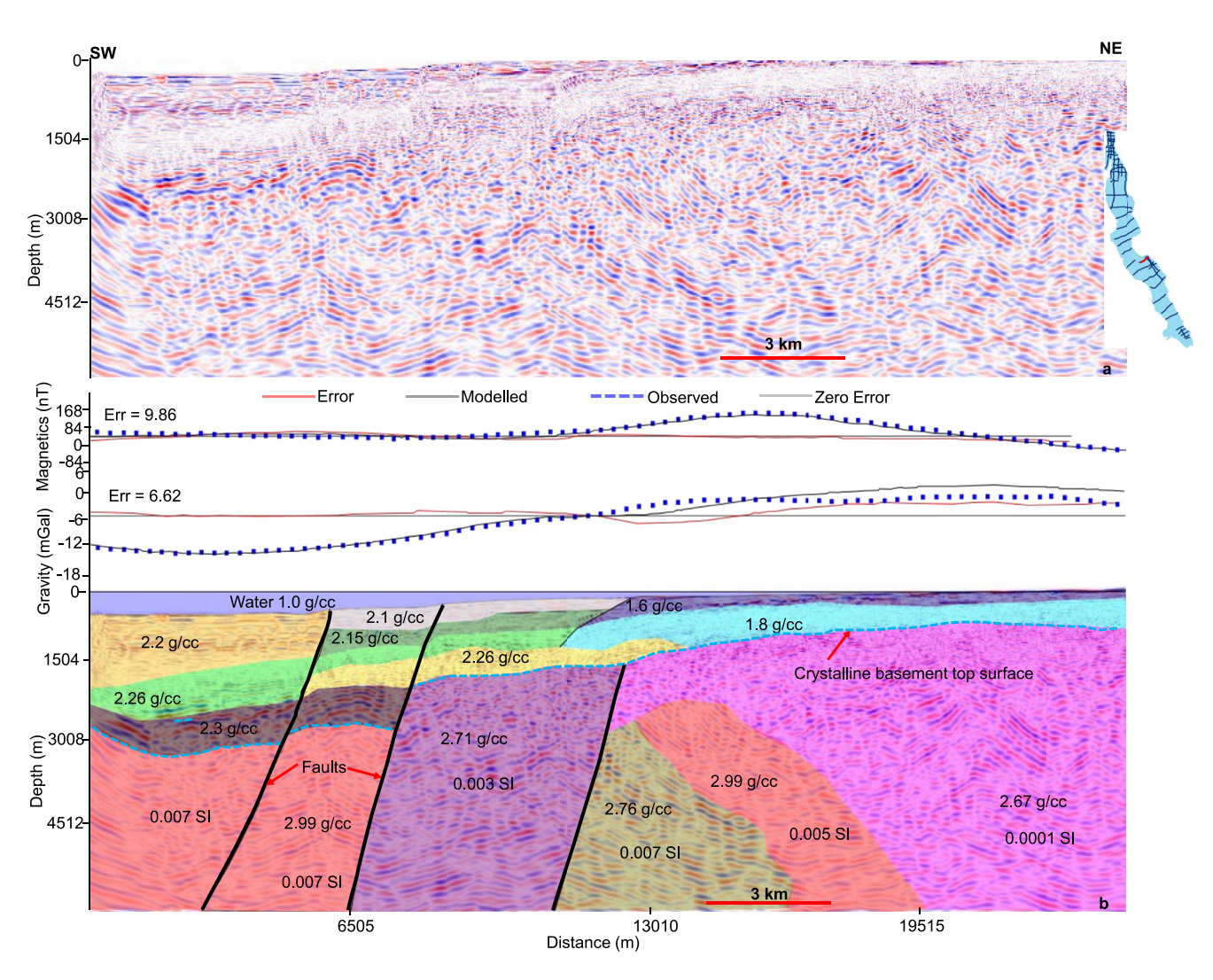


Figure 8. (a) NE-SW PROBE seismic profile 83–80 (see red line transect in the side-inset map in A and in Figure 2) located in the northern parts of the Marungu Province. (b) Forward model of the Gravity (T_z) and Magnetic (residual magnetic intensity) along the seismic profile 83–80. Modeled geology: each colored polygon represents a block of density distinct from its neighboring block. Note the high density (2.99 g/cc) basement and high-density sedimentary rocks (2.3 g/cc), likely representing Mesozoic (Karoo) rift phase units.

However, these Butterworth-filtered aeromagnetic maps and upward-continued gravity maps (Figures S5a and S5b in Supporting Information S1) show N-S and NNE-SSW-trending gradients in the northern sub-basins of the rift. Moderate magnetic anomalies (20-250 nT) are predominantly observed in the northern sub-basins (north of the KIR). The NW-striking KIR is resolved in both long and short wavelength maps (Figures 4b and 4c). The lowest magnetic anomalies (0-178 nT) are predominantly evident from the central part toward the northern part of the survey area (Kigoma Province). Both the analytical signal of the RTP TMI and T_z component of the FTG maps show the NW-SE striking fabrics, possibly representing both the sedimentary and shallow basement fabrics. In addition, a similar structural trend is observed in the south of the Malagarasi Platform.

4.2. Updated Fault Map of the Tanganyika Rift

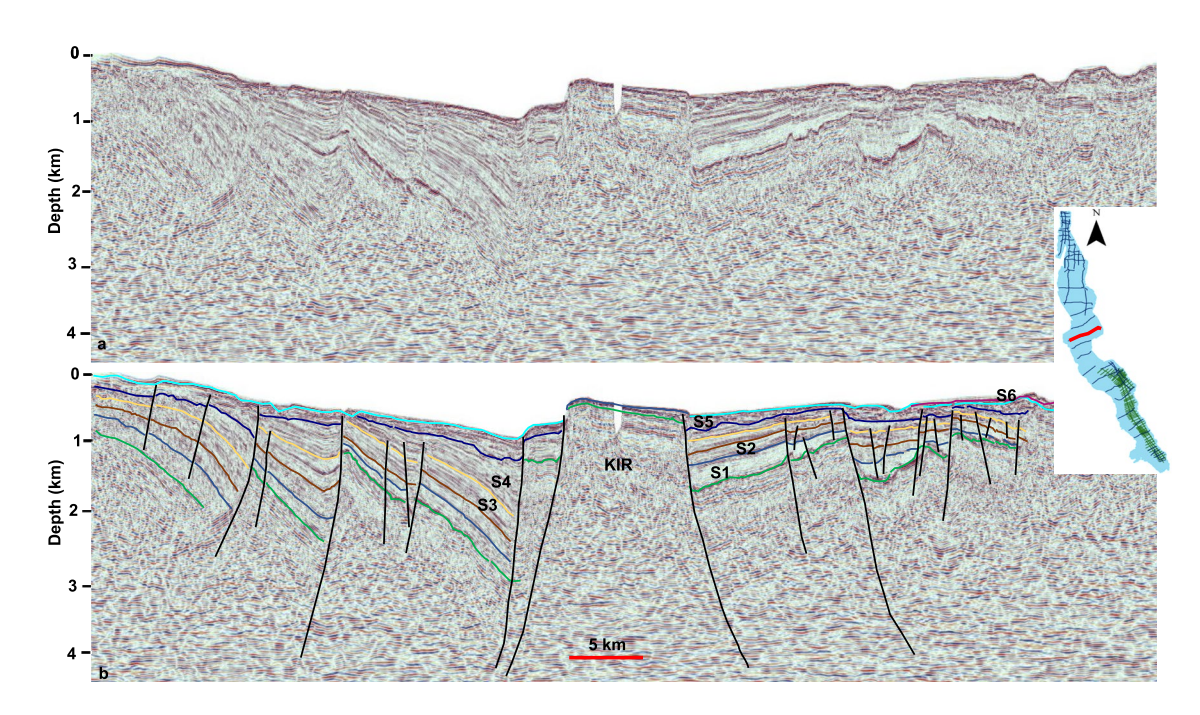
Based on the lineaments extracted from the filtered FTG and aeromagnetic data and their derivatives, we have updated the fault map of the LTR (Figure 6a). There are several of the lineaments that are consistent with faults mapped in Muirhead et al. (2019) and Rosendahl (1987). However, from this study we have confirmed the lateral extent of these previously mapped faults and added additional faults, especially in the Kigoma Province.

Overall, the updated fault map shows that the Tanganyika Rift is dominated by NW-SE trending fault systems. However, a secondary fault set trending NNE-SSW is resolvable, mostly occurring in the northern sub-basins of

SHABAN ET AL. 14 of 28

19449194, 2023, 7, Downloaded from https://agupubs.onlinelibrary.wiley.com/doi/10.10292022TC007726, Wiley Online Library on [04/07/2023]. See the Terms and Conditional Condit

tions) on Wiley Online Library for rules of use; OA articles are governed by the applicable Creative Commons Licens



Tectonics

Figure 9. Seismic dip profile, SW-NE across the Kavala Island Ridge (KIR). (a) Uninterpreted (top) and (b) interpreted (bottom) sections with six identified seismic horizons, from oldest to youngest. Note that the KIR is devoid of sedimentary units except thin unit interpreted to be S1 (or may be S6), implying the active nature of the ridge. The ridge is bounded by two major rift segment border faults with opposing polarities. Sedimentary packages thicken toward these faults implying syn-depositional faulting. Note that across the profile there are two main fault trends. In contrast to seismic unit S1, seismic characteristics of S2-S6 display high amplitude and parallel to semi-parallel reflections suggesting a deeper lake environment.

the rift. The results show the that the dominant fault trends closely correspond to the dominant structural trends in the rotational invariant of the FTG data, further validating the dominance of intra-sedimentary structures in the rotational invariant maps (compare Figures 5c and 5d with Figure 6a rose diagram).

4.3. 2.75-D Models of the Central Tanganyika Rift

The 2.75-D forward modeling along the seismic profile 83–218 (Figures 7a and 7b) reveals previously unresolvable heterogeneities in the crystalline basement underlying the Tanganyika Rift as well as salient features in the sedimentary section. The model permits the inclusion of deep-seated sedimentary rocks with a density of 2.35 and 2.45 g/cc directly overlying the crystalline basement. Generally, the model predicts a sedimentary package with densities varying from 1.8 g/cc in the northeast part of the profile within the youngest unit, and 2.45 g/cc in the central and eastern part of the profile overlying the crystalline basement. It is revealed that sediments in both ends, the northeastern and southwestern parts of the profile, are characterized by low densities. Within shallower seismic units 3–4 (Shaban et al., 2021), a prominent V-shaped intra-sedimentary unit with a density of 2.2 g/cc is resolvable; the discontinuous seismic facies pattern within this unit permits an interpretation of a large axial channel complex.

The model suggests an heterogenous crystalline basement with density varying from 2.5 to 3.2 g/cc and magnetic susceptibility varying from 0.0001 to 0.001. At the basement level, the observed data can only be matched by the inclusion of (a) a laterally extensive shallow basement layer of very low density, possibly corresponding to a fractured weathered basement, and (b) a ~4 km-wide sub-vertical body of similarly low-density near the rift axis, which is flanked by basement of normal density. This central low-density sub-vertical basement body defines the footwall of a large intra-basinal fault that is synthetic to the SW-dipping border fault (Figure 7b). Generally, the basement exhibits an asymmetric geometry, high in the southwestern part, and deepens toward the northeast across the profile. Overall, the sediments thicken toward the east of the profile toward the intra-basinal fault. Also, the magnetic anomaly generally increases toward the east of the profile (in the direction of the eastern border fault).

Both gravity (T_z) and aeromagnetic (TMI) anomalies reveal long-wavelength low frequency anomalies across the profile whereas the T_{xx} anomaly exhibits a short-wavelength high frequency feature toward the southwestern part of the model profile, around the intra-basinal synthetic fault. The aeromagnetic data correlates well with the gravity data

SHABAN ET AL. 15 of 28

9449194, 2023, 7, Downloaded from https

com/doi/10.1029/2022TC007726,

Wiley Online Library on [04/07/2023]. See the Terms and Condit

from the southwestern part of the profile up to a model distance \sim 5,880 m, then from this point southeastwards, these anomalies show a divergent pattern which may be due to the rotation of the transect from a rift-orthogonal trend.

The 2.75-D forward modeling of another seismic profile 83–80, located south of profile 84–218 (Figures 8a and 8b) also predicts heterogeneities in the crystalline basement that are similar to those on profile 84–218. Similar to profile 84–218, the model permits the inclusion of deep-seated high-density sedimentary rocks with a density of 2.3 g/cc directly overlying the crystalline basement. The model predicts a sedimentary package with densities decreasing from the northeast part (1.6 g/cc) to the southwest part of the profile (2.3 g/cc) (Figures 8a and 8b).

The model along profile 83–80 predicts crystalline basement heterogeneities with density varying from 2.67 to 2.99 g/cc and magnetic susceptibility varying from 0.0001 to 0.007. To balance the gravity anomaly at the basement level, the observed data are matched by including a ~4.5 km-wide sub-vertical body of similarly low-density (2.71 g/cc) between high-density bodies (2.99 g/cc). This central low-density sub-vertical basement body defines the footwall of a large intra-basinal fault that is synthetic to the SW-dipping border fault (Figure 7b). Generally, the basement exhibits an asymmetric geometry, high in the southwestern part, and deepens toward the northeast across the profile. Contrary to profile 84–218, overall, the sediments thicken toward the west of the profile. Generally, both the gravity and magnetic anomalies increase in magnitude toward the east of the profile.

4.4. Sedimentation Across the Kavala Island Ridge

The seismic reflection data reveal thin package of seismic facies attributable to the sedimentary package around the crest of the KIR (Figure 9). The sedimentary units on either side of the ridge display a wedge-shape toward the ridge especially in S1, S3, S4, and S5, units. However, S2 unit shows relatively less thickening toward the border faults.

5. Discussion

The augmentation of high-resolution potential field data with 2-D seismic reflection data has helped to constrain the structural characteristics of the central part of the LTR. The potential field data sets help as an infill for areas with only widely spaced seismic reflection data coverage. Basin geometry and basement structures can be interpreted from FTG, and aeromagnetic grid enhancements enable good correlation between anomalies and large structures such as border faults imaged in the seismic reflection data. The analysis reveals faulted basement representing rift zone border faults and intra-basinal faults and reveals changes in the orientation of the lineaments at various depth ranges. This study provides a more precise and detailed structure delineation than previously available, especially in the Kigoma and Kalemie provinces (Tanzania side).

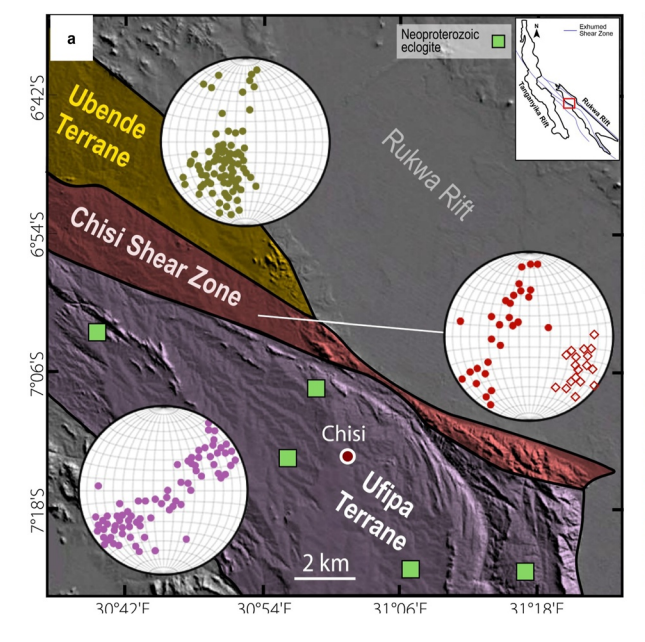
The integration of potential field and seismic data is however limited to the central eastern part of the LTR due to data coverage constraints. Also, the petrophysical properties such as density and magnetic susceptibility used for 2.75D gravity and magnetic modeling have considerable uncertainties (refer to Section 3.4).

5.1. The Pre-Rift Basement Structure Beneath the Tanganyika Rift

The filtered FTG and aeromagnetic data have revealed the dominant NW-trending high density and magnetic fabrics at deeper structural levels, especially in the eastern part of the Kigoma Province, around the boundary between the Kigoma and Kalemie provinces, the eastern part of the Kalemie Province and the central and eastern parts of the Marungu Province (Figures 4 and 5, and Figure S2 in Supporting Information S1). These fabrics highlight the dominant fabrics in the Precambrian metamorphic basement (intermediate and long-wavelength and derivative filters), consistent with the NW-trend of the previously mapped metamorphic fabrics on the rift shoulder onshore (Morley, 1988; Muirhead et al., 2019). The ~4 km-wide, sub-vertical, low-density high magnetic susceptibility body near the rift axis, resolved in the 2.75-D forward models, provide evidence supporting the presence of major sub-vertical structural boundaries in the basement beneath the rift axis. These profiles (Profile 84–218 in the north and 83–80 at about 50 km to the south) show a resolved intra-basement shear zone of similar width (~4 km) potentially representing the same laterally continuous basement shear zone beneath the rift axis. We speculate that this laterally continuous shear zone may possibly represent the offshore continuation of the Kate-Kipili Shear Zone that has been mapped onshore on the Tanganyika Rift flank (Delvaux et al., 2012; Figures 1c and 13).

SHABAN ET AL. 16 of 28

10.1029/2022TC007726



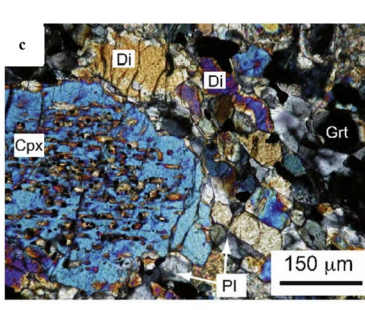


Figure 10. (a) Hillshade map of the eastern rift shoulder of the Tanganyika Rift (see location in Figures 2a and 2b), showing exposures of one of the exhumed NW-trending Precambrian basement shear zones in the region, the Chisi Shear Zone and its bounding basement terranes (modified after Kolawole, Phillips, et al., 2021). The stereographic projections of published field measurements (circles: poles to gneiss foliation planes, diamonds: poles of mineral elongation lineation) show the dominant NW-SE trends of metamorphic fabrics within the shear zone and terranes. (b, c) Outcrop photograph and photomicrograph of eclogites in mylonitic garnet-clinopyroxene gneiss along the shear zone, indicating the presence of a suture zone along the mobile belt (source: Boniface et al., 2012). The photomicrograph shows reaction textures typical of eclogite facies metamorphism. Cpx, Clinopyroxene; Grt, Garnet; Di, Diopside; Pl, Plagioclase.

In map view, we interpret the basement fabrics delineated in the filtered aeromagnetic maps to generally represent basement metamorphic fabrics (i.e., large-scale foliation and ductile shear zones). The shear zones commonly bound the amalgamated basement terranes (e.g., Figures 1c and 10a; Kolawole, Firkins, et al., 2021; Kolawole, Phillips, et al., 2021). The basement shear zone and foliation trends in the basement terranes have also been studied in outcrops along the eastern shoulder of the Tanganyika Rift (Boven et al., 1999). The most prominent of the shear zones is the Chisi Shear Zone (CSZ), a NW-trending >600-km long, 6–12 km-wide shear zone along which eclogite facies metamorphic rocks have been found, suggesting collisional suturing of the terranes (Figures 10a–10c; Boniface et al., 2012; Kolawole, Phillips, et al., 2021). These shear zones have been interpreted to have controlled the geometry and early-rift strain distribution along the neighboring Rukwa Rift (Kolawole, Phillips, et al., 2021). In addition, the shear zones exert a persistent influence on Cenozoic rift faulting in the rift basins (Daly, 1988; Delvaux et al., 2012; Kolawole, Phillips, et al., 2021) and in the zone of interaction between the Rukwa and Tanganyika Rifts (Kolawole, Firkins, et al., 2021). Furthermore, we suggest that the observed NW-SE and NNE-SSW basement fabric trends influenced the Cenozoic NW-SE and NNE-SSW fault trends within the LTR. Several authors have suggested that the reactivation of pre-existing crustal shear zones influenced the rifting, propagation, and linkage of the Cenozoic basins (e.g., Dixey, 1956; McConnell, 1972).

5.2. Incipient Stage of the Tanganyika Rift and the Controls of Structural Inheritance

The investigation of the influence of pre-rift structures on rift evolution along the axis of deep sediment-filled rift basins is challenging as the evolving tectonic deformation and high sedimentation rates often overprint earlier-emplaced rift structures (e.g., Versfelt & Rosendahl, 1989). Here by integrating high-resolution FTG, aeromagnetic data and basin scale 2-D MCS along the rift axis, we are able to evaluate the inheritance of pre-rift structures. The seismically-constrained 2.75-D models presented in this study clearly establish that the pre-rift crystalline basement is heterogeneous, as indicated by variable densities (refer to Section 4.3). There is no basement-penetrating borehole in the region, thus this new information obtained from the FTG survey provides constraints on the deep subsurface basement composition that is not resolvable by the available seismic reflection

SHABAN ET AL. 17 of 28

9449194, 2023, 7, Downloaded from https://agupubs

.com/doi/10.1029/2022TC007726,

Wiley Online Library on [04/07/2023]. See the Terms

articles are governed by the applicable Creative Commons Licens

data. The distribution of basement density and magnetic susceptibility along the modeled profiles is consistent with property values associated primarily with felsic crystalline rocks (2.6–2.75 g/cc density and 100–2,500 micro-cgs susceptibility) with some mafic rocks (density higher than 2.75 g/cc and susceptibility above 3,000 micro-cgs).

Furthermore, our structural mapping of basement aeromagnetic fabrics show that the metamorphic fabrics of the high magnetic susceptibility basement beneath the rift axis are aligned with the dominant trends of the Precambrian shear zones and foliation on basement exposures on the rift flank, and that the rift faults exploited the exhumed basement shear zones. This is supported by the general NNW-SSE and NNE-SSW structural trends identified from the regional aeromagnetic fabrics and foliation in basement exposures as demonstrated in Section 3.1. Also, the NNW -to- NW oriented structures are parallel to the trend of large basement ridges on the rift flank, such as the Mahale Mountains and Katenga–Kugulu–Ntengo (Luama footwall) lineaments, which represent the continuation of the exhumed Precambrian CSZ that extends from the Rukwa Rift through the Tanganyika Rift and Luama Rift (Kolawole, Phillips, et al., 2021). At the regional scale, Dixey (1956), McConnell (1972), and Versfelt and Rosendahl (1989) and Klerkx et al. (1998) suggested that the Cenozoic rifting along the Rukwa-Tanganyika rift zones follow the Proterozoic mobile belts and that the trends rotate around the southwestern margin of the Tanzania craton. More specifically, the NNW striking rift faults follow the fabrics of the Ubdendian and Ufipa terranes whereas the NNE striking rift faults follow the Kibaride fabrics. The studies defined the inherited basement fabrics to include pre-Cenozoic local faults and fractures, axial planar metamorphic fabrics, strike of igneous bodies, metamorphic facies, schistocity and compositional layer boundaries.

Furthermore, Versfelt and Rosendahl (1989) demonstrate that remnants of the Karoo and Cretaceous rift basins in the region appear to be oriented parallel to the trends of major sub-segments of the Tanganyika Rift. The pre-Cenozoic rifts are parallel to the KIR and sub-parallel to the west Kigoma half graben as well as the southern half of the Tanganyika Rift. Furthermore, the gravity and magnetic models predict that the intrabasinal normal fault in seismic profile 218 follows the western edge of the basement anomaly, a ~4 km wide structure, here interpreted as a paleo-shear zone, possibly representing a Precambrian terrane boundary (refer Sections 3.3 and 4.4). This phenomenon provides insight on the possible structural inheritance.

Our analysis suggests three generations of fault development: an older deep NW-SE, NNW-SSE, and NNE-SSW striking fault set controlled by pre-rift basement structures, and although the older set were subsequently reactivated, a younger, shallower ENE-WSW striking set may have later developed. This observation is consistent with previous studies (e.g., Corti et al., 2007; Lezzar et al., 2002). The deep, older faulting occurred during the initial stages of the Rift development, possibly in the Early-mid Miocene. This is evidenced by these faults cutting across the Seismic units 1–5 (Shaban et al., 2021), and contributing to the total rift extension (Morley, 1989; Muirhead et al., 2019; Wright et al., 2020). The orientation of older, deep structures in the LTR closely matches with some exhumed Precambrian mylonitic basement shear zones and fold axes in the northern Malawi Rift (e.g., Kolawole et al., 2018; Tiercelin et al., 1988) and those in the Rukwa Rift (e.g., Kolawole, Phillips, et al., 2021; Wheeler & Karson, 1989).

The prominent magnetic anomaly observed in the southern part of the survey (northern part of the Marungu Province) suggests the presence of a shallow crystalline basement of mafic affinity, possibly overlain by sediments with high magnetic susceptibilities (Figure 3 and Figure S2 in Supporting Information S1). This is supported by our modeling analysis that predicts a crystalline basement with density of 2.99–3.2 g/cc and magnetic susceptibility of up to 0.008, consistent with mafic intrusions possibly associated with Mesozoic Rifting. Given the proximity of the Rungwe Volcano and the presence of Precambrian basement terranes with abundant magnetic minerals, the sediments sourced from these areas are expected to be rich in magnetic minerals. However, it is assumed that the dominant magnetic basement in the rift fill is the pre-rift metamorphic basement. Mafic intrusions are common in the region especially in the Ubendian belt, the Bangweulu craton (Figure 11), and the Archean Greenstone Belt in Tanzania, for example, including the mafic metavolcanics in the Sukumaland Greenstone Belt (Borg & Shackleton, 1997; Manya, 2004) and mafic dykes reported in gold mines (e.g., Eberle, 1988).

Though the thickness of these high-density lithologies for individual terranes within the rift is small, they are pervasive making a large contribution to the whole terrane/rock density. Also, their width size is consistent with the modeled lithologies. For example, looking at Figures 7 and 11, it can be seen that the lateral extent of the ultramafic intrusive is more than 20 km whereas the modeled high-density unit in Figure 7 is approximately 15 km wide. Also, looking at Figures 1c and 11, farther to the south-west of the modeled profiles there are Paleoproterozoic

SHABAN ET AL. 18 of 28

19449194, 2023, 7, Downloaded from https://agupubs.onlinelibrary.wiley.com/doi/10.1029/2022TC007726, Wiley Online Library on [04/07/2023]. See the Terms and Conditions (https://or

articles are governed by the applicable Creative Commons

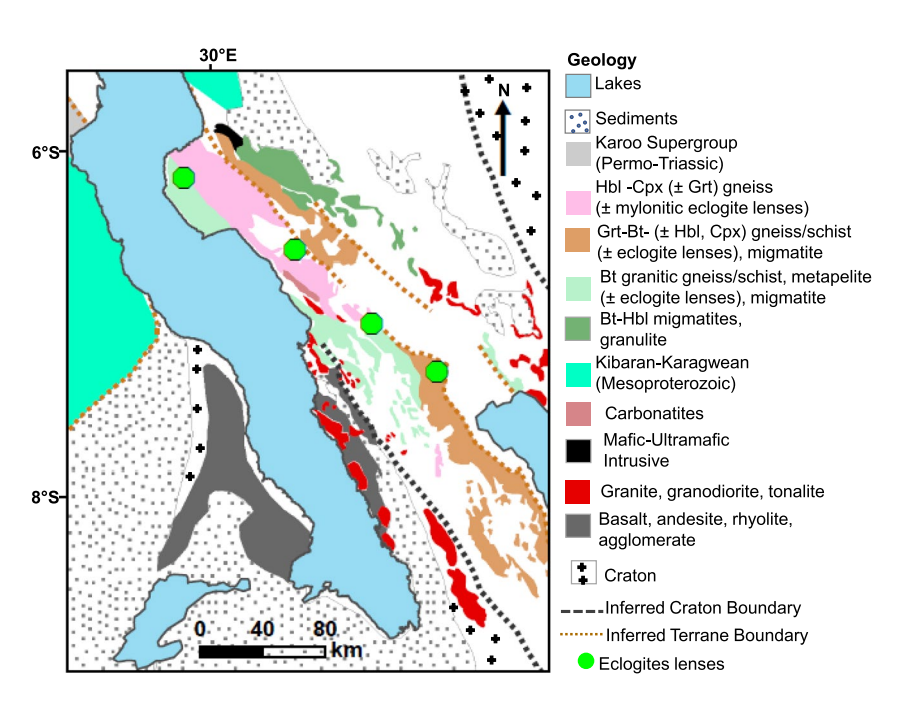


Figure 11. Geological map of the central Ubendian Belt showing the main lithologies in different terranes (modified after Boniface and Tsujimori (2021) and references therein) Bt, biotite; Cpx, clinopyroxene; Grt, garnet; Hbl, hornblende. Note the presence of eclogite and ultramafic rocks attributable to high-density lithologies predicted by the forward models. Note that the terranes boundaries are exhumed ductile shear zones.

magmatic arc units (granites, granodiorites, tonalites, basalts, andesites, rhyolites and agglomerates) which may reach as far north as the modeled profile in Figure 7. The density of tonalite and basalt could be as dense as 3.2 g/cc (Jébrak et al., 1991). The predicted density of 2.9–2.99 g/cc (e.g., Figure 8 and Figures S8 and S9 in Supporting Information S1) is attributable to eclogite facies. It should be noted that, the extent of these magmatic arc units below the lake or sedimentary cover is merely assumed. Therefore, in places like these where the subsurface information is obscured, gravity and magnetics data are useful for discerning the basement structure.

5.2.1. The Presence of Karoo Sediments in the Kalemie-Marungu Provinces

Delvaux (2001) suggested the presence of Permo-Triassic "Karoo" sediments in the Kalemie-Marungu provinces within the Ubendian belt based on the interpretation of multichannel seismic profiles in the LTR by Sander and Rosendahl (1989). They interpreted that the Karoo rift system in the Rukwa-Tanganyika rift was a precursor of the late Cenozoic rifting. However, apart from the outcropping sediments within the Lukuga depression along the Congolese side of Lake Tanganyika, there are no rock samples from the LTR to support the presence of Karoo sediments in the Kalemie-Marungu provinces. Our model predicts the possible presence of sediments below the Nyanja Event (Figure 7) with a density of 2.45 g/cc. This elevated density may be representative of the Karoo sediments buried at least 2.5 km in the subsurface, likely comprised of sandstones, shale, coal, siltstone, and conglomerates (Cahen, 1978; Delvaux, 2001). Using an analogous density of the Karoo sediments in Malawi and Luangwa Basins (i.e., 2.4 g/cc, Peirce & Lipkov, 1988; Matende et al., 2021), our calculated model response considerably matches the observed gravity anomaly (Figure 7b). In addition, our model indicates that the Karoo sediments in this area must have been significantly eroded prior to the Cenozoic rifting because the modeled thickness (i.e., ~300 m) is significantly lower than the Karoo sediments in the adjacent Rukwa Rift which has been estimated to be approximately ~3,500 m thick (Morley et al., 1992; Wescott et al., 1991). However, the maps of Karoo half-grabens in this region show that they were very much restricted in size, suggesting limited accommodation for sediment deposition.

5.3. The Kavala Island Ridge and Its Implications

Although the modeled seismic section is located just south of the KIR, being one of the persistent structurally controlled basement ridges in the Tanganyika Rift, we discuss the implications of the ridge for the tectonic and

SHABAN ET AL. 19 of 28

19449194, 2023, 7, Downloaded from https://agupubs.onlinelibrary.wiley.com/doi/10.1029/2022TC007726, Wiley Online Library on [04/07/2023]. See the Terms

for rules of use; OA articles are governed by the applicable

geomorphic evolution of the rift. The KIR is the most prominent rift segment boundary in the entire LTR and arguably the entire western branch of the EARS, and this high block has been an important physiographic and limnological barrier through much of the history of Lake Tanganyika. From our analysis, magnetic anomalies and FTG intermediate and long wavelength anomalies suggest that a major tectonic lineation intersects the rift around the KIR, parallel to sub-parallel to the NNW striking regional basement foliation (Figures 3 and 4, Figures S2 and S5 in Supporting Information S1). Kolawole, Phillips, et al. (2021) suggested that to the northwest, the CSZ splays into two branches as it intersects the Tanganyika Rift in which one continues into the Luama Rift's northeast footwall via the KIR, and the other rotates northwards into the northern part of the Kigoma Province. However, based on our filtered aeromagnetic map (Figure S7 in Supporting Information S1), our preferred interpretation is that the CSZ extends into the northern part of the Kigoma province, and less likely into the footwall of the Luama Rift. Whereas the splay that continues into the Luama Rift's northeast footwall via the KIR is a different Precambrian Shear Zone, herein referred to as Mahale-Katenga Shear Zone.

Major shear zones are inferred to strongly control the structural evolution of the LTR system. The oblique intersection of a laterally propagating rift tip at a pre-rift shear zone may induce stress redistribution at the rift tip (Crane & Bonatti, 1987). We propose that the Tanganyika Rift was initially segmented across the exhumed Mahale-Katenga Shear Zone during which the southern tip of the Kigoma Province is deflected along the shear zone. This resulted in the formation of the Kigoma and Kalemie graben sub-basins and the KIR. We suggest that subsequent interaction and strain transfer between the Kalemie and Kigoma grabens across the KIR led to the linkage and coalescence of the rift basins and drowning of the KIR. Pre-rift crustal scale shear zones have been suggested to transiently arrest or deflect the lateral propagation of rift segments and associated faults. For instance, the rift-oblique/orthogonal Sanangoe and Lurio shear zones have been suggested to temporarily terminate and subsequently refract the lateral propagation of the Shire Rift Zone in the EARS, as evidenced by the termination of its early-phase rift tips near the shear zones (Kolawole et al., 2022). Also, the NW-striking Precambrian Aswa Shear Zone terminates the Western Branch of the EARS north of the Albertine-Rhino Graben (Katumwehe et al., 2015, 2016). The halting of unilateral rift propagation by such crustal-scale mechanical barriers result in the development of a "locked zone" at the rift tip (Kolawole et al., 2022; Van Wijk & Blackman, 2005).

Considering the long-term prominence and persistence of the KIR as a topographic high in the middle of this ancient lake, we highlight its evolutionary history in the context of rift faulting, rift propagation, paleoclimate and paleogeography of the region. Tectonic displacement along the faulted margins of the KIR is due to the southern and northern extensions of the Kigoma and Kalemie structural province border faults, respectively (Figures 1a, 9, and 12). Seismic reflection data (Figure 11) show that the crest of the KIR is nearly devoid of sedimentary units except for a thin part of S1 unit and possibly S6 units. The sedimentary units on either side of the ridge display a wedge-shape toward the ridge especially in S1, S3, S4, and S5, units, suggesting that the ridge was active during the deposition of these units. We suggest that the KIR growth initiated during the first stage of rifting, as major border faults in the Kigoma and Kalemie structural provinces attained nearly their full present length early in the Cenozoic rift history (Morley, 1989). During the deposition of S2 unit there was decrease in tectonic strain along the faults bounding the KIR, as evidenced by is relatively less significant thickening of the S2 unit toward the border faults. From the S3 to S5 deposition period, the bounding faults of the KIR reactivated, as indicated by the thickening of the sedimentary packages toward the ridge (Figure 12). S6, which has a constant thickness away from the ridge, represents the sedimentary drape from the latest highstand phase of Lake Tanganyika (e.g., Scholz et al., 2007).

We attribute the large (\sim 40 km long and 8 km wide) lineament striking almost N-S in the northeastern part of the Kigoma Province to high-density sedimentary rocks or shallow basement on the platform. Based on wavelength analysis on the T_z anomaly, the anomaly seems to have grown on top of the pre-existing basement high relief, and the platform is within 3 km of the lake surface (Figure S6 in Supporting Information S1). In conjunction with the KIR, these two lineaments together with the Kigoma border fault control how the Malagarasi River delivers sediments into the lake. Consequently, the Malaragasi channel passes between these two lineaments, and eventually deposits sediments north of the KIR and west of the NNE-SSE platform. This interpretation is supported by the work of Shaban et al. (2021) that identified channel complex deposits in these localities attributed to the Malargarasi River drainage system. The drainage morphology of the Malargarasi and Lugufu rivers indicate modern tilting of the Malagarasi Platform along the border fault of the Kigoma Province.

In summary, the KIR developed along a large and long exhumed paleo-Precambrian ductile shear zone in the basement, possibly representing an offshore continuation of known Precambrian shear zones onshore on the rift

SHABAN ET AL. 20 of 28

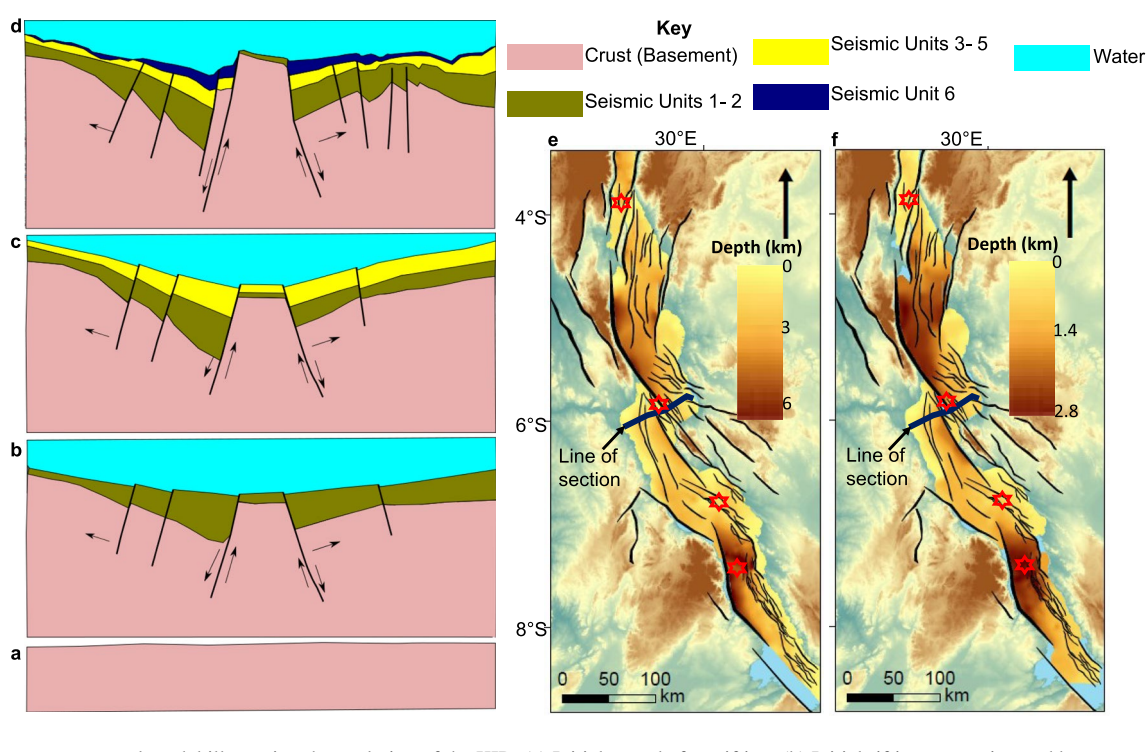


Figure 12. Summary conceptual model illustrating the evolution of the KIR. (a) Initial stage before rifting. (b) Initial rifting stage triggered by two major faults with opposing polarities. During this stage, deposition of thicker units 1–2 was contemporaneous with the ridge evolution. (c) Mid-rifting stage. Seismic units 3–5 were deposited during this period contemporaneous with the ridge evolution, (d) Late stage of KIR evolution. Note that the ridge was uplifted higher, and some of the sediments were eroded from the top of the ridge. (e) Structure contour map (in depth) of the Nyanja Event horizon, the deepest, regionally mappable pre-rift surface (Muirhead et al., 2019; Rosendahl, 1987; Shaban et al., 2021). This horizon corresponds to the green reflector at the base of S1 in Figures 2c and 2d. (f) Structure contour map (in depth) of the horizon at top of S3 unit, a syn-rift unit at intermediate depths.

flank. We suggest that this exhumed paleo-shear zone may have acted as a mechanical barrier during the southward propagation of the northern Tanganyika Rift, thus defining a "locked zone" during the earlier rift phase. The KIR block subsequently became brittly deformed and drowned beneath the modern lake as the lake level rose. However, the relatively high relief of the KIR created a persistent elevated ridge in the rift floor of the central Tanganyika Rift, modulating the patterns of sedimentation in the area over repeated dry and wet paleoclimatic cycles. The present-day stratigraphic patterns atop and around the KIR suggests that the high and frequent lowstand lake level exposures eroded most of the sedimentary section atop the crest of the ridge.

5.4. The Persistent Influence of Incipient Rift Structure on Subsequence Rift Phases

From our 2.75-D modeling, we show that the interpreted axial channel complex is bounded by the localized intra-basinal high and the eastern border fault. The persistent intra-basin high block observed adjacent to the early-rift intra-basin fault is also observed on the structural map of top of seismic deposition unit 3 (Shaban et al., 2021; Figure 9) and is co-located with the broad topographic high along the modern lake floor in the Kalemie Sub-Basin (Figures 5 and 13, Figure S6 in Supporting Information S1). Based on the analysis of basement lineaments in this study, it is evident that topographic highs along the modern lake floor are associated with deep structural highs along the rift axis in the earliest syn-rift units (Figure 12). Prominent topographic highs, interpreted as accommodation zones are commonly associated with large border faults, including the KIR, the Burton's Bay Ridge that separates the Kigoma and Ruzizi provinces, and the Moba high that separates the Kalemie and Marungu province (Rosendahl, 1987; Rosendahl et al., 1986; Shaban et al., 2021). We suggest that during the initial stage of the rift evolution, some of the pre-existing basement fabrics such as shear zones accommodate strain, and normal faulting occurs by preferentially following the pre-existing weaknesses. During the middle stage of rift evolution, the intra-basinal fault that originally exploited pre-existing fabrics continued to localize tectonic strain. Then, during the latest stage of the rift evolution, as sediments deposition continued, the sediments covered the abandoned intra-basin fault, producing a subtle bathymetric high over the older footwall block (Figure 13c). Differential compaction of sediments on top of the buried intra-basinal fault likely contributed

SHABAN ET AL. 21 of 28

1949194, 2023, 7, Downloaded from https://agupubs.onlinelibary.viley.com/doi/10.1029/2022TC007726, Wiley Online Library on [04/07/2023]. See the Terms and Conditions (https://onlinelibrary.wiley.com/terms-and-conditions) on Wiley Online Library for rules of use; OA articles are governed by the applicable Creative Commons

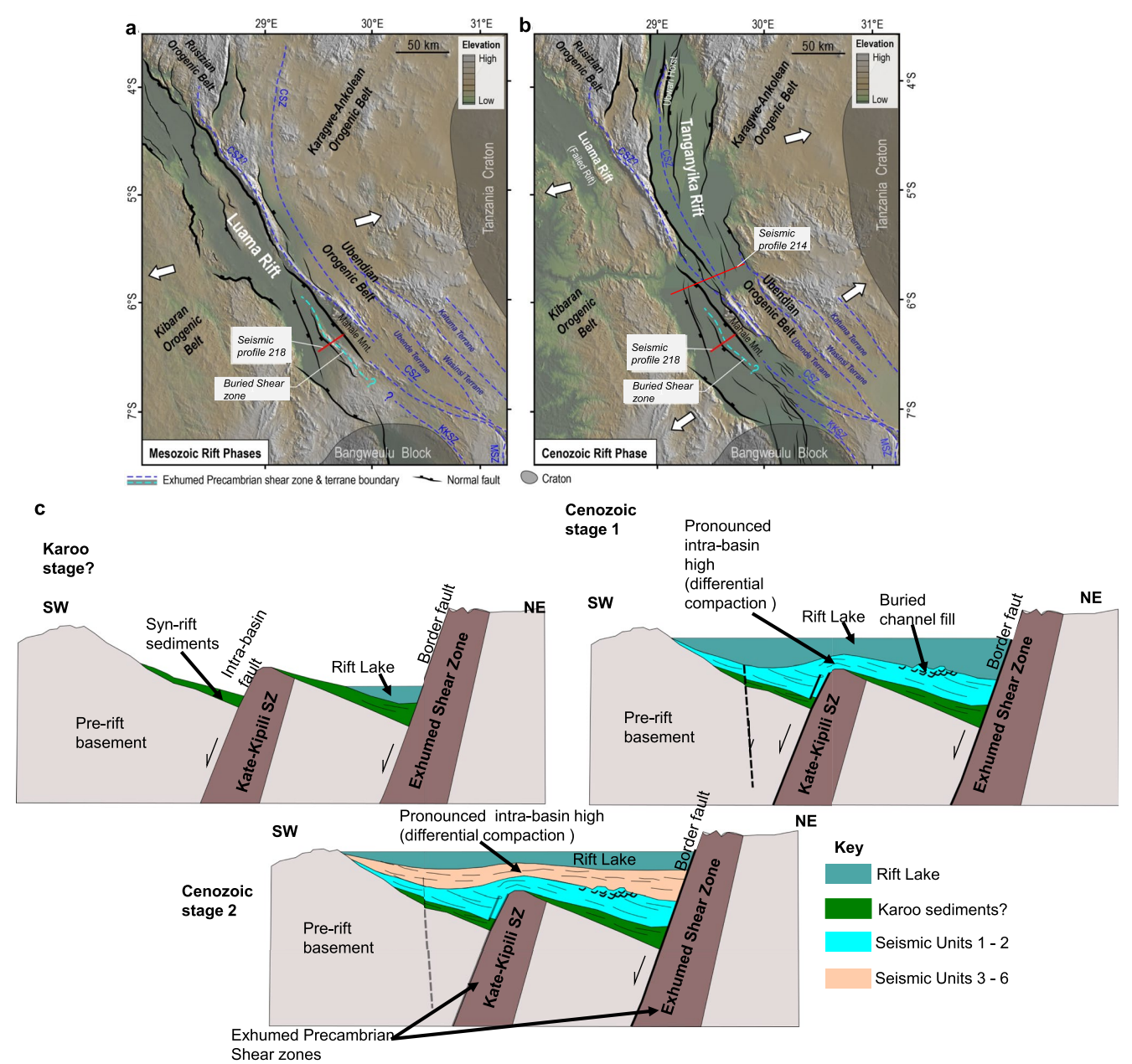


Figure 13. (a) Interpretation of paleo-topography of southwest Tanzania and eastern Congo during the Pre-Cenozoic phases of tectonic extension in East Africa (i.e., Karoo and Cretaceous). The map also shows the pre-rift basement shear zones (previously published ones and those mapped in this study) and rift-related faults. Paleo-extension direction is from Delvaux et al. (2012). (b) Present-day topography of the region showing faults along the evolving Tanganyika Rift. Note that the map includes both the currently active and dormant faults along the Tanganyika Rift. We interpret that the earliest faults in the central Tanganyika Rift (Kalemie Sub-basin) represent the south-eastern extension of the Luama Rift (see Figure 7 seismic section and forward model). Extension directions are from Delvaux (2001) and Delvaux and Barth (2010). Exhumed basement shear zones are from Daly (1988), Delvaux et al. (2012), and Kolawole, Phillips, et al. (2021). CSZ, Chisi Shear Zone; KKSZ, Kate-Kipili Shear Zone; MSZ, Mtose Shear Zone. (c) Cartoons illustrating the interpreted structural and landscape evolution of the Central Tanganyika Rift, highlighting the persistent influence of the incipient rift structure (Stage 1) on the subsequent rift basin architecture (Stages 2 and 3).

to the modern relief. Such topographic highs and differential compaction structures can form potential hydrocarbons traps in rift systems (e.g., Hao et al., 2009).

These observations indicate that the structures of the Mesozoic rifting phase played an important role in localizing upper crustal deformation during Cenozoic phase of the rift evolution. In other parts of the western branch of the rift system, recent studies have also highlighted the roles of earlier rift phase faulting in focusing deformation during the subsequent rift phases. For example, in the Shire Rift Zone of southern Malawi—western

SHABAN ET AL. 22 of 28

19449194, 2023, 7, Downloaded from https

agupubs.onlinelibrary.wiley.com/doi/10.1029/2022TC007726,

Wiley Online Library on [04/07/2023]. See the Terms

on Wiley Online Library for rules of use; OA articles are governed by the applicable Creative Commons Licens

Mozambique, some of the faults of the Mesozoic rift phases localized border and intra-basinal faulting during the Cenozoic phase of rifting (Castaing, 1991; Kolawole et al., 2022). Ojo et al. (2022) used low temperature apatite fission-track cooling histories to show that the reactivated faults in the Shire Rift sustained significant tectonic activity since the Late Oligocene through Miocene. Also, faulting patterns of the earliest Mesozoic rift phase in the Rukwa Rift, controlled by pre-rift basement metamorphic fabrics, remain persistent into the current phase of extension (Kolawole, Phillips, et al., 2021), Further, using satellite DEM and aeromagnetic data, Heilman et al. (2019) showed that progressive southeastward unilateral propagation of some of Rukwa Rift's early-phase faults are facilitating hard-linkage between Rukwa and North Malawi Rift segments.

6. Conclusions

Here, we integrated new high-resolution aeromagnetic, Air-FTG, and seismic reflection data to assess the deep basin and underlying basement structure of the central LTR, East Africa. The short-wavelength, high-frequency components of the FTG and aeromagnetic data provided insights into the shallow structural fabrics, corresponding to intra-sedimentary depth intervals, and the longer-wavelength, lower-frequency components to discern the deeper basement structural fabrics. Furthermore, we forward-modeled multiple rift-perpendicular profiles of the aeromagnetic and gravity data sets that are 40–50 km apart, constrained by the seismic reflection data, to illuminate the broad composition of the basement and the deepest sedimentary units along the rift axis.

The results show a dominance of NW and NNE-trending fabrics within the shallow depths, consistent with the dominant trends of rift faults mapped in the seismic reflection data. The deeper basement is dominated by NW-trending fabrics, consistent with the dominant trend of exhumed basement shear zones and strike of metamorphic foliation in basement terranes along the rift shoulder. These results demonstrate the large-scale control of inherited basement fabrics on the geometry of rift faulting along the central Tanganyika Rift, potentially extending to the northernmost and southernmost parts of the rift basin.

These analyses support long held concepts that a major intra-basinal ridge, the KIR developed along a large exhumed paleo-Precambrian ductile shear zone in the basement, possibly representing an offshore continuation of a known Precambrian ductile shear zone exposed onshore on the rift flank. We suggest this exhumed paleo-shear zone may have acted as a mechanical barrier during the southward propagation of the northern Tanganyika Rift, defining a "locked zone" during the earlier rift phases. Seismic interpretations reveal that the relatively high relief of the KIR has been present since its bounding faults were fully established in the early stage of rifting. Tectonic activity on those bounding faults increased in the subsequent phases of the rift evolution, although the high and frequent lowstand lake level exposures eroded most of the sedimentary section atop the crest of the ridge.

The results of our forward models delineated the presence of ~4 km-wide basement-bounded shear zones along the rift axis, which appear to have controlled the location and potentially, the geometry of major early-rift intra-basin fault zones. The shear zones are resolved by low-density and high-magnetic susceptibility blocks that extend from the top-basement surface all the way to the base of the profiles.

Furthermore, we show that the geometry and location of the border fault and largeoffset intra-basin fault, and the anomalously high-density of the deepest sediments on their hanging walls suggest that incipient rifting in the central Tanganyika Rift is likely to be Mesozoic in age. Furthermore, we find that the early-rift structural highs, commonly localized by large-offset intra-basinal faults that exploited exhumed pre-rift basement shear zones, persisted into the subsequent stages of tectonic extension, and in some places continuing to displace the modern lake floor. Altogether, these results highlight that although incipient rift structure may be largely modulated by inherited basement structures, their influence on basin morphology often cascades through to the subsequent stages of tectonic extension.

Data Availability Statement

Data supporting this research are available at the Petroleum Upstream Regulatory Authority of Tanzania and the Tanzania Petroleum Development Corporation (TPDC) with restrictions that require agreements and are not accessible to the public or research community. The data can be accessed upon a formal request to the Petroleum Upstream Regulatory Authority of Tanzania and the Tanzania Petroleum Development Corporation (TPDC).

SHABAN ET AL. 23 of 28

19449194, 2023, 7, Downloaded from https://agupubs.onlinelibrary.

wiley.com/doi/10.1029/2022TC007726, Wiley Online Library on [04/07/2023]. See the Terms

articles are governed by the applicable Creative Commons

Acknowledgments

We extend our acknowledgments to the Petroleum Upstream Regulatory Authority of Tanzania and the Tanzania Petroleum Development Corporation (TPDC) who provided access to the commercial higher resolution 2D multichannel seismic data, FTG and aeromagnetic data that were used for this study. This work was supported by Syracuse University; National Science Foundation (NSF)-Empower Program; and the Tanzania Petroleum Development Corporation. Decision-Space software was provided to Syracuse University through a software grant from Landmark-Haliburton to CAS. We thank the members of the Lacustrine Basin Research Group at SU for their assistance provided while completing this study, particularly Jacqueline Corbett.

References

- Alken, P., Thébault, E., Beggan, C. D., Amit, H., Aubert, J., Baerenzung, J., et al. (2021). International geomagnetic reference field: The thirteenth generation. *Earth Planets and Space*, 73(1), 1–25. https://doi.org/10.1186/s40623-020-01288-x
- Andersen, L. S., & Unrug, R. (1984). Geodynamic evolution of the Bangweulu block, northern Zambia. *Precambrian Research*, 25(1–3), 187–212. https://doi.org/10.1016/0301-9268(84)90032-9
- Baker, B. H. (1971). Explanatory note on the structure of the southern part of the African rift system. Tectonics of Africa, 6, 543-548.
- Baranov, V. (1957). A new method for interpretation of aeromagnetic maps: Pseudo-gravimetric anomalies. *Geophysics*, 22(2), 359–382. https://doi.org/10.1190/1.1438369
- Beacom, L. E., Holdsworth, R. E., McCaffrey, K. J. W., & Anderson, T. B. (2001). A quantitative study of the influence of pre-existing compositional and fabric heterogeneities upon fracture-zone development during basement reactivation. *Geological Society, London, Special Publications*, 186(1), 195–211. https://doi.org/10.1144/gsl.sp.2001.186.01.12
- Biggs, J., Anthony, E. Y., & Ebinger, C. J. (2009). Multiple inflation and deflation events at Kenyan volcanoes, East African Rift. *Geology*, 37(11), 979–982. https://doi.org/10.1130/G30133A.1
- Boniface, N., Schenk, V., & Appel, P. (2012). Paleoproterozoic eclogites of MORB-type chemistry and three Proterozoic orogenic cycles in the Ubendian Belt (Tanzania): Evidence from monazite and zircon geochronology, and geochemistry. *Precambrian Research*, 192, 16–33. https://doi.org/10.1016/j.precamres.2011.10.007
- Boniface, N., Schenk, V., & Appel, P. (2014). Mesoproterozoic high-grade metamorphism in pelitic rocks of the northwestern Ubendian belt: Implication for the extension of the Kibaran intra-continental basins to Tanzania. *Precambrian Research*, 249, 215–228. https://doi.org/10.1016/j.precamres.2014.05.010
- Boniface, N., & Tsujimori, T. (2021). New tectonic model and division of the Ubendian-Usagaran belt, Tanzania: A review and in-situ dating of eclogites.
- Borg, G., & Shackleton, R. M. (1997). The Tanzania and ne-zaire cratons. Oxford Monographs on Geology and Geophysics, 35, 608-619.
- Boven, A., Theunissen, K., Sklyarov, E., Klerkx, J., Melnikov, A., Mruma, A., & Punzalan, L. (1999). Timing of exhumation of a high-pressure mafic granulite terrane of the Paleoproterozoic Ubende belt (West Tanzania). *Precambrian Research*, 93(1), 119–137. https://doi.org/10.1016/s0301-9268(98)00101-6
- Burgess, C. F., Rosendahl, B. R., Sander, S., Burgess, C. A., Lambiase, J., Derksen, S., & Meader, N. (1989). The structural and stratigraphic evolution of Lake Tanganyika: A case study of continental rifting. In *Developments in geotectonics* (Vol. 22, pp. 859–881). Elsevier. https://doi.org/10.1016/b978-0-444-42903-2.50040-3
- Butterworth, S. (1930). On the theory of filter amplifiers. Wireless Engineer, 7(6), 536-541.
- Cahen, L. (1978). Synthèse des connaissances relatives au Groupe (anciennement Série) de la Lukuga (Permien du Zaire).
- Capart, A. (1952). Exploration hydrobiologique du Lac Tanganyika (1946–1947), Resultats scientifiques-Crustacés, Décapods, Brachyures. Institut Royal des Sciences Naturelles de Belgique, 3(3), 41–67.
- Castaing, C. (1991). Post-Pan-African tectonic evolution of South Malawi in relation to the Karroo and recent East African rift systems. *Tectono-physics*, 191(1–2), 55–73. https://doi.org/10.1016/0040-1951(91)90232-h
- Chisenga, C., Kolawole, F., Rajaonarison, T., Atekwana, E. A., Yan, J., & Shemang, E. M. (2023). Localization of large intraplate earthquakes along faulted density-contrast boundaries: Insights from the 2017 Mw6. 5 Botswana earthquake. *Journal of African Earth Sciences*, 197, 104752. https://doi.org/10.1016/j.jafrearsci.2022.104752
- Chorowicz, J. (2005). The east African rift system. Journal of African Earth Sciences, 43(1-3), 379-410. https://doi.org/10.1016/j.jafrearsci.2005.07.019
- Choubert, G., Faure-Muret, A., & Sougy, J. (1968). International tectonic map of Africa 1: 5,000,000, sheet 1. Association of African Geological Surveys.
- Cohen, A. S., Soreghan, M. J., & Scholz, C. A. (1993). Estimating the age of formation of lakes: An example from Lake Tanganyika, East African Rift system. *Geology*, 21(6), 511–514. https://doi.org/10.1130/0091-7613(1993)021<0511:etaofo>2.3.co;2
- Corti, G., Maestrelli, D., & Sani, F. (2022). Large-to local-scale control of pre-existing structures on continental rifting: Examples from the Main Ethiopian Rift, East Africa. Frontiers in Earth Science, 10, 46. https://doi.org/10.3389/feart.2022.808503
- Corti, G., van Wijk, J., Cloetingh, S., & Morley, C. K. (2007). Tectonic inheritance and continental rift architecture: Numerical and analogue models of the East African Rift system. *Tectonics*, 26(6), TC6006. https://doi.org/10.1029/2006tc002086
- Coulter, G. W. (1963). Hydrological changes in relation to biological production in southern Lake Tanganyika. Limnology & Oceanography, 8(4), 463–477. https://doi.org/10.4319/lo.1963.8.4.0463
- Crane, K., & Bonatti, E. (1987). The role of fracture zones during early Red Sea rifting: Structural analysis using space Shuttle radar and LAND-SAT imagery. *Journal of the Geological Society*, 144(3), 407–420. https://doi.org/10.1144/gsjgs.144.3.0407
- Daly, M. C. (1988). Crustal shear zones in Central Africa: A kinematic approach to Proterozoic tectonics. Episodes Journal of International Geoscience, 11(1), 5–11. https://doi.org/10.18814/epiiugs/1988/v11i1/003
- Daly, M. C., Chorowicz, J., & Fairhead, J. D. (1989). Rift basin evolution in Africa: The influence of reactivated steep basement shear zones. Geological Society, London, Special Publications, 44(1), 309–334. https://doi.org/10.1144/gsl.sp.1989.044.01.17
- Daly, M. C., Klerkx, J., Nanyaro, J. T., & Cognita, T. (1985). Early Proterozoic terranes and strike-slip accretion in the Ubendian Belt of southwest Tanzania. *Terra Cognita*, 5, 257.
- Delvaux, D. (2001). Tectonic and palaeostress evolution of the Tanganyika-Rukwa-Malawi rift segment, East African rift System. *Peri-Tethys Memoir*. 6, 545–567.
- Delvaux, D., & Barth, A. (2010). African stress pattern from formal inversion of focal mechanism data. *Tectonophysics*, 482(1–4), 105–128. https://doi.org/10.1016/j.tecto.2009.05.009
- Delvaux, D., Kervyn, F., Macheyeki, A. S., & Temu, E. B. (2012). Geodynamic significance of the TRM segment in the East African Rift (W-Tanzania): Active tectonics and paleostress in the Ufipa plateau and Rukwa basin. *Journal of Structural Geology*, 37, 161–180. https://doi.org/10.1016/j.jsg.2012.01.008
- Dickinson, J. L., Murphy, C. A., & Robinson, J. W. (2010). Analysing full tensor gravity data with intuitive imaging techniques. In 72nd EAGE conference and exhibition incorporating SPE EUROPEC 2010 (cp-161). European Association of Geoscientists & Engineers.
- Dixey, F. (1956). The East African Rift System. Overseas Geological Mineral Resources Bulletin Supplementary, 1, 1–71.
- Dixon, T. H., Stern, R. J., & Hussein, I. M. (1987). Control of Red Sea rift geometry by Precambrian structures. *Tectonics*, 6(5), 551–571. https://doi.org/10.1029/tc006i005p00551

SHABAN ET AL. 24 of 28

19449194, 2023, 7, Downloaded from https

onlinelibrary.wiley.com/doi/10.1029/2022TC007726,

Wiley Online Library on [04/07/2023]. See

articles are governed by the applicable Creative

- Duchesne, J. C., Liégeois, J. P., Deblond, A., & Tack, L. (2004). Petrogenesis of the Kabanga–Musongati layered mafic—ultramafic intrusions in Burundi (Kibaran belt): Geochemical, Sr–Nd isotopic constraints and Cr–Ni behaviour. *Journal of African Earth Sciences*, 39(3–5), 133–145. https://doi.org/10.1016/j.jafrearsci.2004.07.055
- Eberle, D. (1988). Basic geophysical aspects of gold prospection in Nyanzian greenstone belts of Tanzania. In Open-fi2e Report, 86.
- Ebinger, C. J. (1989). Tectonic development of the western branch of the East African rift system. *Geological Society of America Bulletin*, 101(7), 885–903. https://doi.org/10.1130/0016-7606(1989)101%3C0885:tdotwb%3E2.3.co;2
- Ebinger, C. J., Oliva, S. J., Pham, T. Q., Peterson, K., Chindandali, P., Illsley-Kemp, F., et al. (2019). Kinematics of active deformation in the Malawi rift and Rungwe volcanic province, Africa. *Geochemistry, Geophysics, Geosystems*, 20(8), 3928–3951. https://doi.org/10.1029/2019gc008354
- Evjen, H. M. (1936). The place of the vertical gradient in gravitational interpretations. Geophysics, 1(1), 127–136. https://doi.org/10.1190/1.1437067
 Felton, A. A., Russell, J. M., Cohen, A. S., Baker, M. E., Chesley, J. T., Lezzar, K. E., et al. (2007). Paleolimnological evidence for the onset and termination of glacial aridity from Lake Tanganyika, Tropical East Africa. Palaeogeography, Palaeoclimatology, Palaeoecology, 252(3–4), 405–423. https://doi.org/10.1016/j.palaeo.2007.04.003
- Fernandez-Alonso, M., & Theunissen, K. (1998). Airborne geophysics and geochemistry provide new insights in the intracontinental evolution of the Mesoproterozoic Kibaran belt (Central Africa). *Geological Magazine*, 135(2), 203–216. https://doi.org/10.1017/s0016756898008310
- Florio, G. (2018). Mapping the depth to basement by iterative rescaling of gravity or magnetic data. *Journal of Geophysical Research: Solid Earth*, 123(10), 9101–9120. https://doi.org/10.1029/2018jb015667
- Furman, T. (2007). Geochemistry of East African rift basalts: An overview. Journal of African Earth Sciences, 48(2–3), 147–160. https://doi.org/10.1016/j.jafrearsci.2006.06.009
- Gawthorpe, R. L., & Leeder, M. R. (2000). Tectono-sedimentary evolution of active extensional basins. *Basin Research*, 12(3–4), 195–218. https://doi.org/10.1046/j.1365-2117.2000.00121.x
- George, R., Rogers, N., & Kelley, S. (1998). Earliest magmatism in Ethiopia: Evidence for two mantle plumes in one flood basalt province. Geology, 26(10), 923–926. https://doi.org/10.1130/0091-7613(1998)026%3C0923:emieef%3E2.3.co;2
- Geology, 26(10), 923–926. https://doi.org/10.1130/0091-7613(1998)026%3C0923:emieef%3E2.3.co;2
 Gillespie, P. A., Walsh, J. T., & Watterson, J. (1992). Limitations of dimension and displacement data from single faults and the consequences for
- data analysis and interpretation. *Journal of Structural Geology*, 14(10), 1157–1172. https://doi.org/10.1016/0191-8141(92)90067-7 Grauch, V. J. S., & Hudson, M. R. (2011). Aeromagnetic anomalies over faulted strata. *The Leading Edge*, 30(11), 1242–1252. https://doi.org/10.1190/1.3663396
- Hao, F., Zhou, X., Zhu, Y., & Yang, Y. (2009). Mechanisms for oil depletion and enrichment on the Shijiutuo uplift, Bohai Bay basin, China. AAPG Bulletin, 93(8), 1015–1037. https://doi.org/10.1306/04140908156
- Heilman, E., Kolawole, F., Atekwana, E. A., & Mayle, M. (2019). Controls of basement fabric on the linkage of rift segments. *Tectonics*, 38(4), 1337–1366. https://doi.org/10.1029/2018tc005362
- Hussein, H. M., Marzouk, I., Moustafa, A. R., & Hurukawa, N. (2006). Preliminary seismicity and focal mechanisms in the southern Gulf of Suez: August 1994 through December 1997. *Journal of African Earth Sciences*, 45(1), 48–60. https://doi.org/10.1016/j.jafrearscj.2006.01.006
- Jackson, D., Helwig, J. H., Dinkelman, M. G., Silva, M. & Protacio, J. A. P. (2013). Integration of 2D seismic, gravity gradiometry, and magnetic data on a passive margin-NE Greenland. In 75th EAGE conference & exhibition incorporating SPE EUROPEC 2013 (cp-348). European Association of Geoscientists & Engineers.
- Jacobsen, B. H. (1987). A case for upward continuation as a standard separation filter for potential-field maps. Geophysics, 52(8), 1138–1148. https://doi.org/10.1190/1.1442378
- Jamaludin, S. N. F., Pubellier, M., & Sautter, B. (2021). Shallow vs. deep subsurface structures of Central Luconia province, offshore Malaysia reveal by aeromagnetic, airborne gravity and seismic data. Applied Sciences, 11(11), 5095. https://doi.org/10.3390/appl1115095
- Jébrak, M., LeQuentrec, M. F., Mareschal, J. C., & Blais, D. (1991). A gravity survey across the Bourlamaque massif, southeastern Abitibi greenstone belt, Québec, Canada: The relationship between the geometry of tonalite plutons and associated gold mineralization. *Precambrian Research*, 50(3-4), 261–268. https://doi.org/10.1016/0301-9268(91)90024-5
- Jess, S., Koehn, D., Fox, M., Enkelmann, E., Sachau, T., & Aanyu, K. (2020). Paleogene initiation of the Western branch of the East African Rift: The uplift history of the Rwenzori Mountains, Western Uganda. Earth and Planetary Science Letters, 552, 116593. https://doi.org/10.1016/j.epsl.2020.116593
- Katumwehe, A. B., Abdelsalam, M. G., & Atekwana, E. A. (2015). The role of pre-existing Precambrian structures in rift evolution: The Albertine and Rhino grabens, Uganda. *Tectonophysics*, 646, 117–129. https://doi.org/10.1016/j.tecto.2015.01.022
- Katumwehe, A. B., Abdelsalam, M. G., Atekwana, E. A., & Laó-Dávila, D. A. (2016). Extent, kinematics and tectonic origin of the Precambrian Aswa Shear Zone in eastern Africa. *Gondwana Research*, 34, 241–253. https://doi.org/10.1016/j.gr.2015.03.007
- Katz, B. J. (1990). Lacustrine basin exploration. Case studies and modern Analogs (Vol. 50, p. 340). American Association of Petroleum Geologists, Memoir.
- Kinabo, B. D., Atekwana, E. A., Hogan, J. P., Modisi, M. P., Wheaton, D. D., & Kampunzu, A. B. (2007). Early structural development of the Okayango rift zone. NW Botswana. *Journal of African Earth Sciences*, 48(2–3), 125–136. https://doi.org/10.1016/j.iafrearsci.2007.02.005
- Klerkx, J., Theunissen, K., & Delvaux, D. (1998). Persistent fault controlled basin formation since the Proterozoic along the Western branch of the East African Rift. *Journal of African Earth Sciences*, 26(3), 347–361. https://doi.org/10.1016/s0899-5362(98)00020-7
- Kokonyangi, J. W., Kampunzu, A. B., Armstrong, R., Yoshida, M., Okudaira, T., Arima, M., & Ngulube, D. A. (2006). The Mesoproterozoic Kibaride belt (Katanga, SE DR Congo). *Journal of African Earth Sciences*, 46(1–2), 1–35. https://doi.org/10.1016/j.jafrearsci.2006.01.017
- Kolawole, F., Atekwana, E. A., Laó-Dávila, D. A., Abdelsalam, M. G., Chindandali, P. R., Salima, J., & Kalindekafe, L. (2018). Active deformation of Malawi rift's north basin Hinge zone modulated by reactivation of preexisting Precambrian Shear zone fabric. *Tectonics*, 37(3), 683–704. https://doi.org/10.1002/2017tc004628
- Kolawole, F., Firkins, M. C., Al Wahaibi, T. S., Atekwana, E. A., & Soreghan, M. J. (2021). Rift interaction zones and the stages of rift linkage in active segmented continental rift systems. Basin Research, 33(6), 2984–3020. https://doi.org/10.1111/bre.12592
- Kolawole, F., Phillips, T. B., Atekwana, E. A., & Jackson, C. A. L. (2021). Structural inheritance controls strain distribution during early continental rifting, Rukwa rift. Frontiers in Earth Science, 9, 670. https://doi.org/10.3389/feart.2021.707869
- Kolawole, F., Vick, T., Atekwana, E. A., Laó-Dávila, D. A., Costa, A. G., & Carpenter, B. M. (2022). Strain localization and migration during the pulsed lateral propagation of the Shire Rift Zone, East Africa. *Tectonophysics*, 839, 229499. https://doi.org/10.1016/j.tecto.2022.229499
- Lambiase, J. J. (1990). A model for tectonic control of lacustrine stratigraphic sequences in continental Rift Basins: Chapter 16 (pp. 265–276). https://doi.org/10.1306/m50523c16
- Lambiase, J. J., & Bosworth, W. P. (1995). Structural development and stratigraphy of the Kyokpo Pull-Apart Basin, South Korea and tectonic implications for inverted extensional basins. *Geological Society, London, Special Publications*, 88(1), 457–471. https://doi.org/10.1144/GSL. SP 1995 088 01 24

SHABAN ET AL. 25 of 28

9449194, 2023, 7, Downloaded from https

.com/doi/10.1029/2022TC007726,

Wiley Online Library

on [04/07/2023]. See

articles are governed by the applicable Creative

- Laó-Dávila, D. A., Al-Salmi, H. S., Abdelsalam, M. G., & Atekwana, E. A. (2015). Hierarchical segmentation of the Malawi Rift: The influence of inherited lithospheric heterogeneity and kinematics in the evolution of continental rifts. *Tectonics*, 34(12), 2399–2417. https://doi.org/10.1002/2015tc003953
- Lenoir, J. L., Liégeois, J. P., Theunissen, K., & Klerkx, J. (1994). The Palaeoproterozoic Ubendian shear belt in Tanzania: Geochronology and structure. *Journal of African Earth Sciences*, 19(3), 169–184. https://doi.org/10.1016/0899-5362(94)90059-0
- Lezzar, K. E., Tiercelin, J. J., Le Turdu, C., Cohen, A. S., Reynolds, D. J., Le Gall, B., & Scholz, C. A. (2002). Control of normal fault interaction on the distribution of major Neogene sedimentary depocenters, Lake Tanganyika, East African rift. AAPG Bulletin, 86(6), 1027–1059.
- Livingstone, D. A. (1965). Sedimentation and the history of water level change in Lake Tanganyika. Limnology & Oceanography, 10(4), 607–610. https://doi.org/10.4319/lo.1965.10.4.0607
- Logatchev, N. A., & Zorin, Y. A. (1992). Baikal rift zone: Structure and geodynamics. Tectonophysics, 208(1–3), 273–286. https://doi.org/10.1016/B978-0-444-89912-5.50020-X
- Lonergan, L., Cartwright, J., & Jolly, R. (1998). The geometry of polygonal fault systems in Tertiary mudrocks of the North Sea. *Journal of Structural Geology*, 20(5), 529–548. https://doi.org/10.1016/s0191-8141(97)00113-2
- Malin, K. H. (2017). Improved Constraint on Salt Geometry in the Southern Nordkapp Basin-Modeling salt geometry using potential field data integrated with traditional reflection seismic and well data (Master's thesis, NTNU).
- Manya, S. (2004). Geochemistry and petrogenesis of volcanic rocks of the Neoarchaean Sukumaland greenstone belt, northwestern Tanzania. Journal of African Earth Sciences, 40(5), 269–279. https://doi.org/10.1016/j.jafrearsci.2004.12.006
- Mataragio, J., & Kieley, J. (2009). Application of full tensor gradient invariants in detection of intrusion-hosted sulphide mineralization: Implications for deposition mechanisms. First Break, 27(7), 95–98. https://doi.org/10.3997/1365-2397.27.1301.29032
- Matende, K. N., Atekwana, E., Mickus, K., Abdelsalam, M. G., Atekwana, E. A., Evans, R., et al. (2021). Crustal and thermal structure of the Permian–Jurassic Luangwa–Lukusashi–Luano rift, Zambia: Implications for strain localization in magma–poor continental rifts. *Journal of African Earth Sciences*, 175, 104090. https://doi.org/10.1016/j.jafrearsci.2020.104090
- McConnell, R. B. (1972). Geological development of the rift system of eastern Africa. Geological Society of America Bulletin, 83(9), 2549–2572. https://doi.org/10.1130/0016-7606(1972)83[2549:gdotrs]2.0.co;2
- McGlue, M. M., Ivory, S. J., Stone, J. R., Cohen, A. S., Kamulali, T. M., Latimer, J. C., et al. (2020). Solar irradiance and ENSO affect food security in Lake Tanganyika, a major African inland fishery. Science Advances, 6(41), eabb2191. https://doi.org/10.1126/sciadv.abb2191
- McGlue, M. M., Lezzar, K. E., Cohen, A. S., Russell, J. M., Tiercelin, J. J., Felton, A. A., et al. (2008). Seismic records of late Pleistocene aridity in Lake Tanganyika, tropical East Africa. *Journal of Paleolimnology*, 40(2), 635–653. https://doi.org/10.1007/s10933-007-9187-x
- Mickus, K. L., Aiken, C. L., & Kennedy, W. D. (1991). Regional-residual gravity anomaly separation using the minimum-curvature technique. Geophysics, 56(2), 279–283. https://doi.org/10.1190/1.1443041
- Geophysics, 56(2), 279–283. https://doi.org/10.1190/1.1443041

 Miller, H. G., & Singh, V. (1994). Potential field tilt—A new concept for location of potential field sources. *Journal of Applied Geophysics*,
- 32(2-3), 213-217. https://doi.org/10.1016/0926-9851(94)90022-1
 Mohr, P. A., & Wood, C. A. (1976). Volcano spacings and lithospheric attenuation in the Eastern Rift of Africa. Earth and Planetary Science
- Mohr, P. A., & Wood, C. A. (1976). Volcano spacings and lithospheric attenuation in the Eastern Rift of Africa. Earth and Planetary Science Letters, 33(1), 126–144. https://doi.org/10.1016/0012-821X(76)90166-7
- Mono, J. A., Ndougsa-Mbarga, T., Bi-Alou, M. B., Ngoh, J. D., & Owono, O. U. (2018). Inferring the subsurface basement depth and the contact locations from aeromagnetic data over Loum-Minta Area (Centre-East Cameroon). *International Journal of Geosciences*, 9(7), 435–459. https://doi.org/10.4236/iig.2018.97028
- Morley, C. K. (1988). Variable extension in Lake Tanganyika. Tectonics, 7(4), 785-801. https://doi.org/10.1029/tc007i004p00785
- Morley, C. K. (1989). Extension, detachments, and sedimentation in continental rifts (with particular reference to East Africa). *Tectonics*, 8(6), 1175–1192. https://doi.org/10.1029/TC008i006p01175
- Morley, C. K. (1999). How successful are analogue models in addressing the influence of pre-existing fabrics on rift structure? *Journal of Structural Geology*, 21(8–9), 1267–1274. https://doi.org/10.1016/s0191-8141(99)00075-9
- Morley, C. K. (2002). Evolution of large normal faults: Evidence from seismic reflection data. AAPG Bulletin, 86. https://doi.org/10.1306/61eedbfc-173e-11d7-8645000102c1865d
- Morley, C. K. (2010). Stress re-orientation along zones of weak fabrics in rifts: An explanation for pure extension in 'oblique' rift segments? Earth and Planetary Science Letters, 297(3-4), 667-673. https://doi.org/10.1016/j.epsl.2010.07.022
- Morley, C. K. (2017). The impact of multiple extension events, stress rotation and inherited fabrics on normal fault geometries and evolution in the Cenozoic rift basins of Thailand. *Geological Society, London, Special Publications*, 439(1), 413–445. https://doi.org/10.1144/sp439.3
- Morley, C. K., Cunningham, S. M., Harper, R. M., & Wescott, W. A. (1992). Geology and geophysics of the Rukwa Rift, East Africa. *Tectonics*, 11(1), 69–81. https://doi.org/10.1029/91tc02102
- Morley, C. K., Haranya, C., Phoosongsee, W., Pongwapee, S., Kornsawan, A., & Wonganan, N. (2004). Activation of rift oblique and rift parallel pre-existing fabrics during extension and their effect on deformation style: Examples from the rifts of Thailand. *Journal of Structural Geology*, 26(10), 1803–1829. https://doi.org/10.1016/j.jsg.2004.02.014
- Morley, C. K., Nelson, R. A., Patton, T. L., & Munn, S. G. (1990). Transfer zones in the East African rift system and their relevance to hydrocarbon exploration in rifts. AAPG Bulletin, 74(8), 1234–1253. https://doi.org/10.1306/0c9b2475-1710-11d7-8645000102c1865d
- Muirhead, J. D., Wright, L. J., & Scholz, C. A. (2019). Rift evolution in regions of low magma input in East Africa. Earth and Planetary Science Letters, 506, 332–346. https://doi.org/10.1016/j.epsl.2018.11.004
- Nelson, R. A., Patton, T. L., & Morley, C. K. (1992). Rift-segment interaction and its relation to hydrocarbon exploration in continental rift systems. AAPG Bulletin, 76(8), 1153–1169.
- O'Donnell, J. P., Adams, A., Nyblade, A. A., Mulibo, G. D., & Tugume, F. (2013). The uppermost mantle shear wave velocity structure of eastern Africa from Rayleigh wave tomography: Constraints on rift evolution. *Geophysical Journal International*, 194(2), 961–978. https://doi.org/10.1093/gji/ggt135
- Ojo, O. O., Ohenhen, L. O., Kolawole, F., Johnson, S. G., Chindandali, P. R., Atekwana, E. A., & Laó-Dávila, D. A. (2022). Under-displaced normal faults: Strain accommodation along an early-stage rift-bounding fault in the Southern Malawi Rift. Frontiers in Earth Science, 10, 846389. https://doi.org/10.3389/feart.2022.846389
- Pasteels, P., Villeneuve, M., De Paepe, P., & Klerkx, J. (1989). Timing of the volcanism of the southern Kivu province: Implications for the evolution of the western branch of the East African Rift system. Earth and Planetary Science Letters, 94(3-4), 353-363. https://doi. org/10.1016/0012-821X(89)90152-0
- Peace, A. L., Welford, J. K., Geng, M., Sandeman, H., Gaetz, B. D., & Ryan, S. S. (2018). Rift-related magmatism on magma-poor margins: Structural and potential-field analyses of the Mesozoic Notre Dame Bay intrusions, Newfoundland, Canada and their link to North Atlantic opening. *Tectonophysics*, 745, 24–45. https://doi.org/10.1016/j.tecto.2018.07.025

SHABAN ET AL. 26 of 28

9449194, 2023, 7, Downloaded from

.com/doi/10.1029/2022TC007726,

Wiley Online Library

articles are governed by the applicable Creative Commons

- Peirce, J. W., & Lipkov, L. (1988). Structural interpretation of the Rukwa rift, Tanzania. Geophysics, 53(6), 824–836. https://doi.org/10.1190/1.1442517
- Phillips, T. B., Jackson, C. A., Bell, R. E., Duffy, O. B., & Fossen, H. (2016). Reactivation of intrabasement structures during rifting: A case study from offshore southern Norway. *Journal of Structural Geology*, 91, 54–73. https://doi.org/10.1016/j.jsg.2016.08.008
- Pilkington, M., & Roest, W. (1992). Draping aeromagnetic data in areas of rugged topography. Journal of Applied Geophysics, 29(2), 135–142. https://doi.org/10.1016/0926-9851(92)90004-5
- Ring, U. (1994). The influence of preexisting structure on the evolution of the Cenozoic Malawi rift (East African rift system). *Tectonics*, 13(2), 313–326. https://doi.org/10.1029/93tc03188
- Ring, U. W. E., Schwartz, H. L., Bromage, T. G., & Sanaane, C. (2005). Kinematic and sedimentological evolution of the Manyara Rift in northern Tanzania, East Africa. *Geological Magazine*, 142(4), 355–368. https://doi.org/10.1017/s0016756805000841
- Roberts, E. M., Stevens, N. J., O'Connor, P. M., Dirks, P. H. G. M., Gottfried, M. D., Clyde, W. C., et al. (2012). Initiation of the western branch of the East African Rift coeval with the eastern branch. *Nature Geoscience*, 5(4), 289–294. https://doi.org/10.1038/ngeo1432
- Rosendahl, B. R. (1987). Architecture of continental rifts with special reference to East Africa. *Annual Review of Earth and Planetary Sciences*, 15(1), 445–503. https://doi.org/10.1146/annurev.ea.15.050187.002305
- Rosendahl, B. R., Kilembe, E., & Kaczmarick, K. (1992). Comparison of the Tanganyika, Malawi, Rukwa, and Turkana rift zones from analyses of seismic reflection data. *Tectonophysics*, 213(1–2), 235–256. https://doi.org/10.1016/0040-1951(92)90261-4
- Rosendahl, B. R., Reynolds, D. J., Lorber, P. M., Burgess, C. F., McGill, J., Scott, D., et al. (1986). Structural expressions of rifting: Lessons from Lake Tanganyika, Africa. Geological Society, London, Special Publications, 25(1), 29–43. https://doi.org/10.1144/GSL.SP.1986.025.01.04
- Russell, J. M., Barker, P., Cohen, A., Ivory, S., Kimirei, I., Lane, C., et al. (2020). ICDP workshop on the Lake Tanganyika scientific drilling project: A late Miocene–present record of climate, rifting, and ecosystem evolution from the world's oldest tropical lake. Scientific Drilling, 27, 53–60. https://doi.org/10.5194/sd-27-53-2020
- Salem, A., Williams, S., Fairhead, D., Smith, R., & Ravat, D. (2008). Interpretation of magnetic data using tilt-angle derivatives. Geophysics, 73(1), L1–L10. https://doi.org/10.1190/1.2799992
- Sander, S., & Rosendahl, B. R. (1989). The geometry of rifting in Lake Tanganyika, East Africa. *Journal of African Earth Sciences*, 8(2–4), 323–354. https://doi.org/10.1016/s0899-5362(89)80031-4
- Saria, E., Calais, E., Stamps, D. S., Delvaux, D., & Hartnady, C. J. H. (2014). Present-day kinematics of the East African Rift. Journal of Geophysical Research: Solid Earth, 119(4), 3584–3600. https://doi.org/10.1002/2013jb010901
- Scholz, C. A., Cohen, A. S., Johnson, T. C., King, J. W., & Moran, K. (2006). The 2005 Lake Malawi scientific drilling project. *Scientific Drilling*, 2, 17–19. https://doi.org/10.5194/sd-2-17-2006
- Scholz, C. A., Johnson, T. C., Cohen, A. S., King, J. W., Peck, J. A., Overpeck, J. T., et al. (2007). East African megadroughts between 135 and 75 thousand years ago and bearing on early-modern human origins. *Proceedings of the National Academy of Sciences*, 104(42), 16416–16421. https://doi.org/10.1073/pnas.0703874104
- Scholz, C. A., King, J. W., Ellis, G. S., Swart, P. K., Stager, J. C., & Colman, S. M. (2003). Paleolimnology of Lake Tanganyika, East Africa, over the past 100 kyr. *Journal of Paleolimnology*, 30(2), 139–150. https://doi.org/10.1023/a:1025522116249
- Scholz, C. A., & Rosendahl, B. R. (1988). Low lake stands in Lakes Malawi and Tanganyika, East Africa, delineated with multifold seismic data. Science, 240(4859), 1645–1648. https://doi.org/10.1126/science.240.4859.1645
- Scholz, C. A., Rosendahl, B. R., & Scott, D. L. (1990). Development of coarse-grained facies in lacustrine rift basins: Examples from East Africa. Geology, 18(2), 140–144. https://doi.org/10.1130/0091-7613(1990)018<0140:docgfi>2.3.co;2
- Scholz, C. A., Shillington, D. J., Wright, L. J., Accardo, N., Gaherty, J. B., & Chindandali, P. (2020). Intrarift fault fabric, segmentation, and basin evolution of the Lake Malawi (Nyasa) Rift, East Africa. *Geosphere*, 16(5), 1293–1311. https://doi.org/10.1130/ges02228.1
- Shaban, S. N., Scholz, C. A., Muirhead, J. D., & Wood, D. A. (2021). The stratigraphic evolution of the Lake Tanganyika Rift, East Africa: Facies distributions and paleo-environmental implications. *Palaeogeography, Palaeoclimatology, Palaeoecology*, 575, 110474. https://doi.org/10.1016/j.palaeo.2021.110474
- Sheriff, R. E. (1977). Limitations on resolution of seismic reflections and geologic detail derivable from them: Section 1. Fundamentals of stratigraphic interpretation of seismic data.
- Sherman, S. I. (1992). Faults and tectonic stresses of the Baikal rift zone. *Tectonophysics*, 208(1–3), 297–307. https://doi.org/10.1016/0040-1951(92)90351-6
- Sklyarov, E. V., Melnikov, A. I., Gladkochub, D. P., Theunissen, K., Klerkx, J., & Mruma, A. (1998). Paleoproterozoic eclogites and garnet pyroxenites of the Ubende Belt (Tanzania). Schweizerische Mineralogische und Petrographische Mitteilungen, 78(2), 257–271.
- Smith, M., & Mosley, P. (1993). Crustal heterogeneity and basement influence on the development of the Kenya Rift, East Africa. *Tectonics*, 12(2), 591–606. https://doi.org/10.1029/92tc01710
- Stuckless, E. (2008). Celtic minerals assessment report discussing geochemistry. Geophysics, and diamond drilling on the Budgell's Harbour property. Central Newfoundland.
- Sutton, J., Watson, J., & James, T. C. (1954). Geological study of the metamorphic rocks of Karema and Kungwe Bay, western Tanganyika.

 Bulletin Geological Survey of Tanganyika, 22, 1–70.
- Tack, L., Liégeois, J. P., Deblond, A., & Duchesne, J. C. (1994). Kibaran A-type granitoids and mafic rocks generated by two mantle sources in a late orogenic setting (Burundi). *Precambrian Research*, 68(3–4), 323–356. https://doi.org/10.1016/0301-9268(94)90036-1
- Tack, L., Wingate, M. T. D., De Waele, B., Meert, J., Belousova, E., Griffin, B., et al. (2010). The 1375 Ma "Kibaran event" in Central Africa: Prominent emplacement of bimodal magmatism under extensional regime. *Precambrian Research*, 180(1–2), 63–84. https://doi.org/10.1016/j.precamres.2010.02.022
- Theunissen, K., Klerkx, J., Melnikov, A., & Mruma, A. (1996). Mechanisms of inheritance of rift faulting in the western branch of the East African Rift, Tanzania. *Tectonics*, 15(4), 776–790. https://doi.org/10.1029/95tc03685
- Tiercelin, J. J., Chorowicz, J., Bellon, H., Richert, J. P., Mwanbene, J. T., & Walgenwitz, F. (1988). East African Rift System: Offset, age and tectonic significance of the Tanganyika-Rukwa-Malawi intracontinental transcurrent fault zone. *Tectonophysics*, 148(3–4), 241–252. https://doi.org/10.1016/0040-1951(88)90133-3
- Tiercelin, J. J., Soreghan, M., Cohen, A. S., Lezzar, K. E., & Bouroullec, J. L. (1992). Sedimentation in large rift lakes: Example from the Middle Pleistocene–Modern deposits of the Tanganyika trough, East African rift system. *Bulletin des Centres de Recherches, Exploration-Production Elf-Aquitaine*, 16, 83–111.
- Van Wijk, J. W., & Blackman, D. K. (2005). Dynamics of continental rift propagation: The end-member modes. *Earth and Planetary Science Letters*, 229(3–4), 247–258. https://doi.org/10.1016/j.epsl.2004.10.039
- Vasuki, Y., Holden, E. J., Kovesi, P., & Micklethwaite, S. (2014). Semi-automatic mapping of geological Structures using UAV-based photogrammetric data: An image analysis approach. Computers & Geosciences, 69, 22–32. https://doi.org/10.1016/j.cageo.2014.04.012

SHABAN ET AL. 27 of 28

19449194, 2023, 7, Downloaded from

.com/doi/10.1029/2022TC007726,

Wiley Online Library on [04/07/2023]. See the Terms

and-conditions) on Wiley Online Library for rules of use; OA articles are governed by the applicable Creative Commons

- Vauchez, A., Barruol, G., & Tommasi, A. (1997). Why do continents break-up parallel to ancient orogenic belts? *Terra Nova*, 9(2), 62–66. https://doi.org/10.1111/j.1365-3121.1997.tb00003.x

 Versfelt, J., & Rosendahl, B. R. (1989). Relationships between pre-rift structure and rift architecture in Lakes Tanganyika and Malawi, East
- Africa. Nature, 337(6205), 354–357. https://doi.org/10.1038/337354a0
 Wedmore, L. N. J., Williams, J. N., Biggs, J., Fagereng, Å., Mphepo, F., Dulanya, Z., et al. (2020). Structural inheritance and border fault reacti-
- vation during active early-stage rifting along the Thyolo fault, Malawi. *Journal of Structural Geology*, 139, 104097. https://doi.org/10.1016/j. jsg.2020.104097
 Wescott, W. A., Krebs, W. N., Engelhardt, D. W., & Cunningham, S. M. (1991). New biostratigraphic age dates from the Lake Rukwa rift basin
- Wescott, W. A., Krebs, W. N., Engelhardt, D. W., & Cunningham, S. M. (1991). New biostratigraphic age dates from the Lake Rukwa rift basir in western Tanzania. AAPG Bulletin, 75(7), 1255–1263.
- Wheeler, W. H., & Karson, J. A. (1989). Structure and kinematics of the Livingstone Mountains border fault zone, Nyasa (Malawi) Rift, southwestern Tanzania. *Journal of African Earth Sciences*, 8(2–4), 393–413. https://doi.org/10.1016/s0899-5362(89)80034-x
- Wilson, J. T. (1966). Did the Atlantic close and then re-open?
- Wilson, R. W., Holdsworth, R. E., Wild, L. E., McCaffrey, K. J. W., England, R. W., Imber, J., & Strachan, R. A. (2010). Basement-influenced rifting and basin development: A reappraisal of post-Caledonian faulting patterns from the North Coast transfer zone, Scotland. *Geological Society, London, Special Publications*, 335(1), 795–826. https://doi.org/10.1144/sp335.32
- Wolfenden, E., Ebinger, C., Yirgu, G., Renne, P. R., & Kelley, S. P. (2005). Evolution of a volcanic rifted margin: Southern Red Sea, Ethiopia. Geological Society of America Bulletin, 117(7–8), 846–864. https://doi.org/10.1130/B25516.1
- Wright, L. J., Muirhead, J. D., & Scholz, C. A. (2020). Spatiotemporal variations in upper crustal extension across the different basement terranes of the Lake Tanganyika Rift, East Africa. *Tectonics*, 39(3), e2019TC006019. https://doi.org/10.1029/2019TC006019
- Yong Technology Inc. (2014). Online Rose Diagram [Software]. GeoRose. Retrieved from http://www.yongtechnology.com/yong-lab/online-rose-diagram/

References From the Supporting Information

- Al-Ibiari, M. G., Ismail, A. A., El-Khafeef, A. A., Basheer, A. A., El-laban, A. M., & Tarek, Y. (2018). Analysis and interpretation of aeromagnetic data for Wadi Zeidun area, Central Eastern Desert, Egypt. Egyptian journal of petroleum, 27(3), 285–293. https://doi.org/10.1016/j.ejpe.2017.04.002
- Arisoy, M. Ö., & Dikmen, Ü. (2013). Edge detection of magnetic sources using enhanced total horizontal derivative of the tilt angle. *Yerbilimleri*, 34(1), 73–82.
- Beiki, M. (2010). Analytic signals of gravity gradient tensor and their application to estimate source location. *Geophysics*, 75(6), I59–I74. https://doi.org/10.1190/1.3493639
- Blake, R. (1995). Potential theory in gravity & magnetic application.
- Cooper, G. R. J., & Cowan, D. R. (2006). Enhancing potential field data using filters based on the local phase. *Computers & Geosciences*, 32(10), 1585–1591. https://doi.org/10.1016/j.cageo.2006.02.016
- Ibraheem, I. M., Gurk, M., Tougiannidis, N., & Tezkan, B. (2018). Subsurface investigation of the Neogene Mygdonian Basin, Greece using magnetic data. *Pure and Applied Geophysics*, 175(8), 2955–2973. https://doi.org/10.1007/s00024-018-1809-x
- Kebede, B., & Mammo, T. (2021). Processing and interpretation of full tensor gravity anomalies of Southern Main Ethiopian Rift. Heliyon, 7(4), e06872. https://doi.org/10.1016/j.heliyon.2021.e06872
- Murphy, C. A. (2004). The Air-FTG airborne gravity gradiometer system. In Airborne gravity (pp. 7-14).
- Salem, A., Masterton, S., Campbell, S., Fairhead, J. D., Dickinson, J., & Murphy, C. (2013). Interpretation of tensor gravity data using an adaptive tile angle method. *Geophysical Prospecting*, 61(5), 1065–1076. https://doi.org/10.1111/1365-2478.12039
- Salem, A., Williams, S., Fairhead, J. D., Ravat, D., & Smith, R. (2007). Tilt-depth method: A simple depth estimation method using first-order magnetic derivatives. The Leading Edge, 26(12), 1502–1505. https://doi.org/10.1190/1.2821934

SHABAN ET AL. 28 of 28